In-situ observation of mitochondrial biogenesis as the early event of apoptosis

Chang-Sheng Shao [1,2], Xiu-Hong Zhou [3], Yu-Hui Miao [4], Peng Wang[1], Qian-Qian Zhang [1,2] and Qing Huang [1,2] *

[1] CAS Key Laboratory of High Magnetic Field and Ion Beam Physical Biology, Hefei Institutes of Physical Science, Chinese Academy of Sciences (CAS), Hefei 230031, China;

[2] Science Island Branch of Graduate School, University of Science and Technology of China, Hefei 230026, China;

[3] Center of Biology, Anhui Agricultural University, Hefei, China;

[4] Department of Medical Oncology, The First Affiliated Hospital of USTC, Division of Life Sciences and Medicine, University of Science and Technology of China, Hefei, China;

***Corresponding author:**

Prof. Qing Huang

Hefei Institutes of Physical Science, Chinese Academy of Sciences, P. O. Box 1138, Hefei 230031, P.R. China

Tel: 86-551-65595261; Fax: 86-551-65595261

E-mail: huangq@ipp.ac.cn

Key words: mitochondrial biogenesis, apoptosis, fluorescent proteins, fluorescence

23 **Graphical abstract**

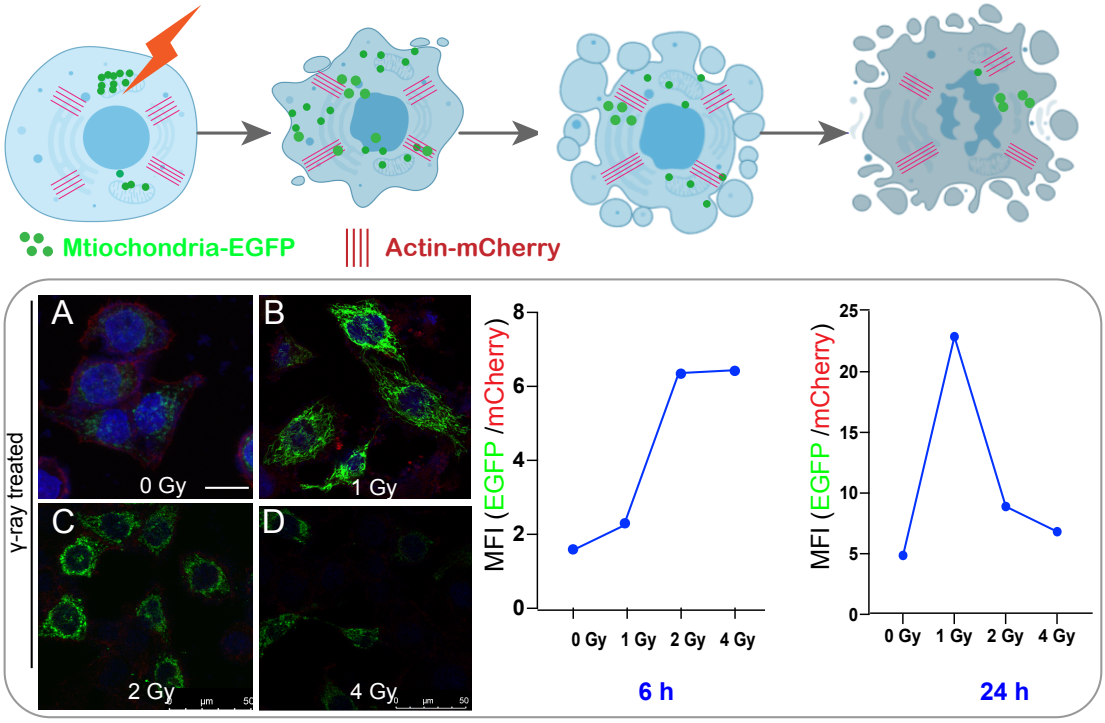

24

Highlights

- A dual fluorescence reporter system was successfully constructed for in-situ observation of mitochondrial biogenesis in living cells.
- The whole process of radiation-induced mitochondrial biogenesis and apoptosis was scrutinized.
- The conception of the relationship between mitochondrial biogenesis and apoptosis was revised.
- Assessment of the early event of mitochondrial biogenesis is critical for prediction of the late fate of cells.

SUMMARY

Mitochondrial biogenesis is a cell response to external stimuli which is generally believed to suppress apoptosis. However, during the process of apoptosis, whether mitochondrial biogenesis occurs in the early stage of the apoptotic cells remains unclear. To address this question, we constructed the COX8-EGFP-ACTIN-mCherry HeLa cells with recombinant fluorescent proteins respectively tagged on the nucleus and mitochondria, and monitored the mitochondrial changes in living cells exposed to gamma-ray radiation. Besides in situ detection of mitochondrial fluorescence changes, we also examined the cell viability, nuclear DNA damage, reactive oxygen species (ROS), Mitochondrial superoxide, citrate synthase activity, ATP, cytoplasmic and mitochondrial calcium, mitochondrial DNA copy number and expression of transcription genes related to mitochondrial biogenesis as well as the apoptosis biomarkers. As a result, we confirmed that significant mitochondrial biogenesis took place preceding the radiation-induced apoptosis, and the change of mitochondrial biogenesis at early time was closely correlated with the apoptotic cells at late stage. The involved mechanism was also discussed.

53 # INTRODUCTION

54 Mitochondrial biogenesis is a physiological response of cells to external stress that
55 may cause increase of energy demand, and it plays an important role in cell metabolism
56 regulation, signal transduction and mitochondrial ROS regulation (Luo et al., 2016;
57 Vyas et al., 2016). Mitochondrial biogenesis maintains cell homeostasis by ensuring the
58 quality of mtDNA and regulating the renewal of organelles (Yambire et al., 2019), and
59 it has been extensively explored in recent years due to the relevant interests in human
60 aging, neurodegenerative diseases, cell metabolic diseases and tumors(Fanibunda et al.,
61 2019).

62 Since mitochondrial regulation plays a very critical role in controlling the cell fate,
63 it is also intriguing for researchers to explore the relationship between mitochondrial
64 biogenesis and apoptosis. Generally, apoptosis is mediated by the activation of the
65 caspase pathways which are associated with mitochondrial damage accompanied by
66 destruction of electron transfer, oxidative phosphorylation, ATP production and change
67 of cell redox potential(Burke, 2017). In fact, some studies have claimed that there is a
68 negative correlation between mitochondrial biogenesis and apoptosis, i.e., apoptosis is
69 normally suppressed by mitochondrial biogenesis. For example, it has been reported
70 that Ca^{2+}-mediated apoptotisis can be inhibited by enhanced mitochondrial biogenesis
71 (Dam et al., 2013), or, on the other hand, apoptosis may occur by inhibiting
72 mitochondrial biogenesis(Cao et al., 2017). Also, in the study of radiation-induced
73 apoptosis, mitochondrial biogenesis was observed and analyzed (Rai et al., 2018), and
74 it was claimed that enhancement of mitochondrial biogenesis could significantly reduce
75 the proportion of apoptosis caused by ionizing radiation(Yu et al., 2013). However,

concerning the whole process of apoptosis, whether and how mitochondrial biogenesis takes place in the early period in the apoptotic cells exposed to the external stimuli such as ionizing radiation remains elusive.

In order to scutinize the relationship between mitochondrial biogenesis and apoptosis, it is thus crucial to monitor the mitochondrial changes in the whole process of apoptotic cells. At present, there are not many methods available to study the influence of external factors on mitochondrial changes. One of the conventional methods is to probe the change of mitochondrial gene copy numbers(Yu, 2011). Another approach is to use fluorescent proteins. Fluorescent proteins are beneficial for studying the living cells with reporting gene expression, which can provide information on protein locations and expression levels as well as the involved biochemical activities(Newman et al., 2011). Actually, study of mitochondrial process using fluorescent proteins is now gaining increasing attention (Katajisto et al., 2015; Melentijevic et al., 2017; Ruan et al., 2017). Recent development is to make use of multiple different fluorescent proteins with different excitation/emission spectra, so that the precision of transcriptional measurements can be ensured by using the reference color for normalization (Miyashiro and Goulian, 2007). In such a circumstance, the ratio of dual fluorescence can be used to eliminate the possible fluorescence measurement errors(Miyashiro and Goulian, 2007). So, with application of this dual fluorescence approach, nowadays researchers are able to observe and analyze the temporal and spatial life trajectories of living cells (Jadhav and Shivdasani, 2019), and

maybe more importantly, to scrutinize the early events leading to various bio-effects such as apoptosis as end-point fate in the living cells (Yu et al., 2020).

Therefore, in the present work, we attempted to apply the dual recombinant fluorescent proteins to monitor the mitochondrial biogenesis induced by injuring radiation, and in this way, to examine whether and how the early event of mitochondrial biogenesis would be related to the prominent bio-effects such as apoptosis. For the effect of radiation as the external stimuli to the cells, it is known that ionizing radiation (such as α-, γ-, X-rays, protons, heavy ions) can readily cause various detrimental damages to living cells, which can lead to the change of genetic information, cell mutations, genomic instability, and apoptosis (O'Driscoll and Jeggo, 2006). Mitochondrion, as the important subcellular organelle, is one of the major targets of ionizing radiation(Leach et al., 2001). On the other hand, radiation can also effectively induce mitochondrial biogenesis (Das et al., 2020). For the establishment of the dual fluorescent system for in-situ observation of mitochondrial biogenesis in living cells, we constructed the stable fluorescent reporter cell lines by lentiviral transfection to achieve mitoGFP and nuclear mCherry. As a result, we fulfilled the task of in-situ and real-time observation of mitochondrial changes in the living cells, and observed the effect of mitochondrial biogenesis occurring in the early process of the apoptotic cells. By analyzing the fluorescence ratio of mitoGFP and nuclear mCherry fluorescence, we could therefore more reliably examine the relationship between the early mitochondrial biogenesis and late apoptosis. The detailed mitochondrial/apoptotic processes were analyzed, and the involved mechanism was discussed.

119 # RESULTS

120 ## Construction of dual-fluorescent stably transfected cell lines

121 In order to construct a universal dual-fluorescence gene reporter vector, we
122 considered to make use of the simplicity of vector construction and referred to the
123 previously reported dual-fluorescence reporter system, and so we chose the CMV
124 promoter to express the dual-fluorescence target proteins. The mitochondrial reporter
125 expression system is generally localized in the stroma, targeting the leader peptide
126 (MSVLTPLLLRGLTGSARRLPVPRAKIHSLGDP) on the VIIIa subunit of
127 cytochrome C oxidase (COX8) (Haggie and Verkman, 2002) (Figure 1A). As such, we
128 constructed the pLVX-mCherry-actin lentiviral vector (Figure 1B).

129 To establish the cell line stably co-expressing COX8-EGFP and ACTIN-mCherry,
130 we transfected the HeLa cells with the plasmid containing the expression sequence of
131 COX8-EGFP, and obtained the COX8-EGFP expression cells. After screening by G418
132 for 2 weeks, the stably transfected cell line was obtained. The COX8-EGFP-mCherry-
133 ACTIN co-expressing HeLa cell line was further established based on the COX8-EGFP
134 expressing cells with lentiviral transfection system. From the as-constructed HeLa cells,
135 we could monitor the cell activities in real time using the living cell workstation. As
136 shown in Figure 1C, with the change of time, we observed the stable expression of GFP
137 located in mitochondrial cytochrome c oxidase, and also confirmed the stable
138 expression of mCherry associated with the actin proteins in the cells. To be noted, the
139 intensity of mCherry fluorescence associated with actin expression was relatively quite

140 constant with the change of time, indicating that actin fluorescence could be applied as
141 the internal standard for the fluorescence reporting system.

142 In order to further confirm the GFP expression right on the targeted mitochondria,
143 we then labeled the mitochondria with TMRE dye in the GFP-tagged cells and then
144 examined the dye-stained cells with a confocal microscope. As shown in Figure 1D, the
145 COX8 protein fluorescence (Green) proteins and mitochondrial fluorescence (Red)
146 were indeed co-localized in the cells.

147 In order to verify the universal validity of our as-constructed dual fluorescence
148 reporting system for observing mitochondrial biogenesis, we also used mitochondrial
149 biogenesis's initiator 5-Aminoimidazole-4-carboxamide ribotide (AICAR) as for the in-
150 depth testing, or, as the positive control (Komen and Thorburn, 2014). The applied drug
151 concentration was 0.5 mM. As shown in the Figures 2A-B, compared with the non-
152 AICAR treatment group, the AICAR treated group showed increased fluorescence ratio
153 with time. This experiment therefore confirmed that the dual fluorescence system we
154 constructed is feasible and effective for monitoring mitochondrial biogenesis.
155 Furthermore, the correlation between GFP and mitochondrial biogenesis related protein
156 expression were also confirmed by the WB assay (Figures 2C-D). We testified the co-
157 expression levels of GFP protein together with the mitochondrial target protein (e.g.
158 COX8) for the cells treated by AICAR. Technically, cytochrome c (CytoC) was
159 measured in the experiment instead of COX8 as COX8 is the subunit of CytoC oxidase.
160 As shown in Fig. 2C, both GFP and CytoC were in the same trend of expression of
161 levels for the mitochondrial biogenesis proteins including PGC1-α, NRF1 and TFAM.

162 Besides, we also examined the AICAR-induced biomarker proteins expression levels
163 related to mitochondrial biogenesis. Figure 2D shows that for the cells treated with
164 AICAR, the expression levels of GFP, CytoC, PGC1-α, NRF1 and TFAM increased
165 significantly in comparison with the untreated group. Also, with the increase of AICAR
166 treatment time, the protein expression levels of mitochondrial biogenesis marker
167 proteins (PGC1, NRF1, TFAM) also increased concomitantly (see Figure S1). All these
168 results therefore confirmed the validity of our fluorescence report system suitable for
169 mitochondrial biogenesis monitoring.
170

171 **In-situ observation of the dual fluorescence reporter system for the evaluation of**
172 **the radiation-induced mitochondrial changes**

173 With the establishment of this dual-fluorescence reporter system, we then employ
174 the laser fluorescence confocal microscope to observe the biological effect in the living
175 cells with the treatment of gamma-ray (γ-ray) irradiation. The COX8-EGFP encoding
176 mitochondria (Green), the ACTIN-mCherry encoding actin (Red), and the DAPI-
177 stained nuclei were observed. The representative images together with the
178 corresponding quantitative analysis of fluorescence intensity are shown in Figure 3A.

179 Figure 3A presents the fluorescent images of the cells by confocal microscopy,
180 indicating that the intracellular mitochondrial content increased with radiation dose.
181 Compared with the control group (0 Gy), the irradiated group showed mitochondrial
182 fluorescence enhancement, and it was significantly enhanced especially for the 1 and 2

183 Gy cases (Figure 3B). The fluorescent images intuitively show that the number of
184 mitochondria increased with increasing radiation dose, confirming that the dual
185 fluorescence reporter system can directly reflect the relevant mitochondrial responses
186 and changes in the living cells.

187 To investigate the mitochondrial fluorescence enhancement of the cells exposed to
188 ionizing radiation, the mean fluorescence intensity (MFI) from the dual fluorescence
189 reporter system was utilized. This MFI ratio change was also obtained by employing
190 the High Content Imaging and Screening (HCS) system, with the results shown in
191 Figure 3C. The HCS living cell workstation recorded the changes of cell fluorescence
192 within 24 hours after cell irradiation (the videos were also recorded, see Videos S1, S2,
193 S3 in the Supporting Information). The results indicate that for 1 Gy, the fluorescence
194 ratio GFP/mCherry increased with time, while for 2 Gy and 4 Gy cases, the
195 fluorescence ratio increased significantly with the irradiation dose during the first
196 interval of 1-12 hours, but afterwards, it decreased to some extent, though still higher
197 than that of the control (non-irradiated cells). The reduction in MFI suggested that the
198 mitochondria of the irradiated cells with higher radiation doses were actually more
199 detrimentally damaged by the radiation than that received lower radiation doses. Figure
200 S2 shows the numerical changes of two fluorescence channels detected by flow
201 cytometry. The MFI ratio of $EGFP^{+}$: $mCherry^{+}$ was calculated, and it was found that
202 the fluorescence ratio was positively correlated with the radiation dose. The result by
203 the flow cytometry (Figure S2) also confirms there were significant differences between
204 the irradiated and non-irradiated groups. To be noted, in order to verify the validity or

205 reliability of actin fluorescence as an internal reference even under the irradiation
206 condition, in-situ observation of real-time fluorescence data were also recorded after
207 irradiation which showed that there was no significant difference in fluorescence
208 expression within 24 hours (Figure S3).

209 **Radiation effect on cell viability, survival rate, cell cycle, apoptosis, DNA damage**
210 **and mitochondrial membrane damage**

211 To investigate the radiation effect, the cell viability was measured by CCK-8
212 method, showing that the cell viability decreased with the increase of radiation dose
213 (Figure 4A). The toxic effect of radiation on cells was also examined using LDH kit,
214 which revealed that the radiation-induced toxicity was indeed increased significantly
215 with radiation dose (Figure 4B). Also, the colony-forming method was used to analyze
216 the inhibitory effect of γ-ray on HeLa cell survival. With increase of γ-ray irradiation
217 dose, the cell survival rate was only 30% after 4 Gy irradiation (Figure 4C), confirming
218 that the cell survival rate decreased with the rise of radiation dose.

219 In addition, the cell cycle and apoptosis were assessed for the cells irradiated with
220 γ-ray. Apoptotic cells were detected by flow cytometry after irradiation using Annexin
221 V-PI methods (Figure 4D). Through statistics and comparison of the number of
222 apoptotic cells, it was found that with the increase of radiation dose, the number of
223 apoptotic cells also increased significantly (Figure 4E). Cell cycle was analyzed by flow
224 cytometry, and the results showed that all groups of cells had G2 arrest after 24 hours

225 of irradiation, especially at 2 Gy and 4 Gy irradiation doses showed significant G2 arrest
226 (Figure 4F).

227 Furthermore, in order to explain the reasons for the radiation effects, the radiation
228 induced damages on DNA and mitochondrial membrane, together with the
229 accompanied cytosolic ROS (cROS) and mitochondrial-ROS (mROS) levels, were also
230 examined, as shown by the results in Figure 5. In the experiments, the
231 immunofluorescence method was used to detect DNA damage, CellROX Green probe
232 was used to label cytosolic ROS, mitoSOX-Red probe was used for mitochondrial ROS
233 level, and JC-1 was used to label mitochondrial membrane potential. Figure 5A shows
234 that with increase of the radiation dose, the cytosolic ROS expression level increased
235 significantly, and the statistical results showed that the ROS level in the irradiated cells
236 increased with the increase of the radiation dose (Figure 5C). At the dose of 2 Gy, the
237 cROS level was the highest, and for the 4 Gy group, there was a significant difference
238 compared with the non-irradiated group. Besides, we also employed a mitochondrial
239 biogenesis inhibitor, namely cyclosporin A (CsA), as for the negative control. Indeed,
240 with the treatment of CsA, the cROS level was significantly increased (Figure 5C).

241 ROS could induce mitochondrial damage, which would further activate the positive
242 feedback circuit, resulting in more ROS production in damaged mitochondria.
243 Therefore, we also used MitoSOX probe to detect mitochondrial ROS (Figure 5B). We
244 observed an insignificant increase in the mitochondrial ROS level with increasing
245 radiation dose compared with that of the control group (Figure 5D). Similarly, after
246 treated with 50 nM CsA, the level of mitochondrial ROS was increased due to the

247 inhibition of mitochondrial biogenesis. To be noted, mROS can be released into the
248 cytoplasm through mitochondrial permeability transition pore (mPTP), which is also an
249 important source of cROS in the cytoplasm. Therefore, we could expect that ionizing
250 radiation would as a result also cause the increase of both mROS and cROS
251 simultaneously.

252 For the mitochondrial damage evaluation, it is known that mitochondrial
253 membrane potential ($\Delta\Psi_m$) is produced by proton pump of electron transport chain,
254 which is necessary for ATP production. Therefore, we also evaluated $\Delta\Psi_m$ using JC-1
255 staining. As shown in Figures 6A-B, the promotion of JC-1 monomers enhanced
256 significantly with the increase of radiation dosage. It was found that $\Delta\Psi_m$ was markedly
257 lower depending on the increased radiation dosage. After CsA (50 nM) treatment, the
258 mitochondrial membrane potential decreased (Figure 6C).

259 As the ionizing radiation induced DSB of DNA, we expected that there would also
260 be enhanced DNA repair process in the irradiated cells. Indeed, we observed the
261 fluorescence from γ-H2AX and the co-localization of 53BP1 foci after the radiation
262 exposure. Figure 7 shows the number of foci increased significantly with the increase
263 of radiation dose, while the number of foci of 53BP1 was the largest at 2 Gy but then
264 decreased with radiation dose, implying that at higher radiation dose the cell received
265 severer damage son the DNA repair ability became weaker.

266 **Verification of mitochondrial calcium and ATP level**

267 Mitochondrial calcium plays a key role in regulating cell homeostasis, which has a

268 dual regulation mechanism. On one hand, mitochondrial calcium can affect cell activity
269 by activating oxidative metabolism, mitochondrial respiration and ATP synthesis. On
270 the other hand, the increase of mitochondrial calcium influx is also one of the
271 inducements of apoptosis and necrosis. In our experiment, we employed a cytoplasmic
272 calcium probe (Fluo-4 AM) and a mitochondrial calcium probe (Rhod-2 AM) to detect
273 the changes of calcium in the cytoplasm and mitochondria, and we obtained the result
274 as shown in Figure 8A, which indicates that with the increase of radiation dose, the
275 fluorescence intensity of Fluo-4 AM and Rhod-2 AM increased significantly. The
276 analysis of the fluorescence intensities shows that the increase of calcium content in
277 cytoplasm and mitochondria was positively correlated with radiation dose (Figures 8B-
278 C). In addition, we treated the cells with CsA, which could inhibit the mitochondrial
279 biogenesis, and the result confirmed that CsA also significantly improved the calcium
280 release in both cytoplasm and mitochondria.

281 The imbalance of calcium homeostasis can further increase the production of
282 reactive oxygen species and trigger the imbalance of mitochondrial energy metabolism
283 (including the release of cytochrome c and apoptosis caused by permeability transition
284 pore). The level of ATP is a marker to detect the level of mitochondrial energy
285 metabolism, so we also detected the expression of ATP in cells at different time points
286 (6, 12, 24 h) with different radiation doses (1 Gy, 2 Gy, 4 Gy). As shown in Figure 9, at
287 each time point, with the increase of radiation dose, intracellular ATP level decreased
288 significantly. For the same radiation dose, the expression level of ATP decreased
289 significantly with the increase of time.

290 ***Verification of mitochondrial biogenesis, apoptosis and mitophagy.***

291 To further verify the mitochondrial biogenesis induced by radiation, the copy
292 number of mitochondrial DNA was evaluated firstly. Total DNA was extracted from
293 HeLa cells 6-24 hours after irradiation. As shown in Figure 10A, the copy number of
294 mitochondrial DNA changed significantly after cell irradiation. Indeed, under the same
295 radiation dose, mitochondrial DNA number increased significantly compared with that
296 of the non-irradiated cells. At 6 and 12 hours, the ratio of mitochondrial DNA to nuclear
297 DNA increased significantly with the increase of irradiation dose. At 24 hours, the ratio
298 was the highest at 1 Gy, and decreased with the increase of radiation dose.

299 Citrate synthase (CS) is the initial enzyme of tricarboxylic acid (TCA) cycle. It
300 exists in almost all cells that can be oxidized and metabolized, and it is also an important
301 exclusive marker of mitochondrial matrix. Since CS enzyme is a key biomarker of
302 mitochondrial biogenesis, we therefore also detected the activity of CS enzyme change
303 after irradiation. As shown in the Figure 10B, at 6 hours, with the increase of radiation
304 dose, CS increased significantly, suggesting that radiation stimulated mitochondrial
305 biogenesis at the early stage. At 24 hours, low dose irradiation (1 Gy) could still increase
306 the activity of CS, while it was reduced at higher radiation doses (2 Gy, 4 Gy),
307 indicating that when the radiation damage became severer, mitochondrial biogenesis
308 would diminish in the late stage of cell process. In addition, we also applied CsA as the
309 inhibitor of mitochondrial biogenesis for the negative control. Indeed, after CsA
310 treatment, the activity of CS decreased, and this decrease was more significant with

311 increase of time.

312 Furthermore, to explore the correlation between mitochondrial biogenesis and
313 apoptosis under the condition of radiation, the related marker proteins were also
314 examined. For the mitochondrial change, the related protein expression levels of PGC-
315 1α, NRF1, TFAM and Mfn1 at different times (6 h, 12 h, 24 h) with different radiation
316 doses (0 Gy, 1 Gy, 2 Gy, 4 Gy) were assessed by Western blots (Figure 10C). At early
317 stage (6 hours) of the process, the expression level of PGC-1α, p-AMPK, TFAM protein
318 was increased with radiation dose. On the other hand, for the apoptosis, the related
319 protein expression levels of apoptosis-related marker proteins (BAX, Bcl-2, CytoC,
320 Caspase-3, Cleaved Caspase-9, PARP) were examined. As shown in Figure 8, the
321 expression levels of crucial apoptosis proteins did not differ significantly at early time
322 (6 h), but their expression levels increased significantly afterwards (12 h, 24 h). So these
323 results unambiguously demonstrate that the mitochondrial biogenesis at early time was
324 positively correlated to the apoptosis in the late stage.

325 So, as shown above, in the early stage after radiation, mitochondrial biosynthesis
326 would be stimulated and increased, but with the lapse of time, for the larger irradiation
327 dose, we found the decrease of mitochondrial energy metabolism (including the
328 decrease of citrate synthase, mitochondrial membrane potential, mitochondrial DNA
329 copy number, etc) and the inhibition of mitochondrial biogenesis. As the mitochondrial
330 damage became severer, we also expected that mitophagy might play an important role
331 to clear up the dysfunctional mitochondria, because mitophagy is an important
332 degradation mechanism to eliminate dysfunctional mitochondria through

333 autophagosomes(Montava-Garriga and Ganley, 2019). Therefore, we examined
334 mitophagy by stably transfecting the mKeima plasmid to target the expression on the
335 mitochondria of HeLa cells. mKeima fluorescent protein can change its excitation
336 wavelength and show different color fluorescence at different pH values. Under pH
337 neutral condition, it can be excited to green fluorescence at 485 nm, while under acidic
338 condition, it can be excited to red fluorescence at 560 nm. We thus evaluated the
339 intensity ratio of 560 nm to 485 nm fluorescence bands to determine the occurrence of
340 mitophagy. As shown in Figure 11A, the ratio increased significantly with the increase
341 of radiation dose, suggesting that at higher radiation dose mitophagy became dominant.
342 AICAR, as a stimulant of mitochondrial biogenesis (positive control), also induced
343 mitophagy, while CsA as an inhibitor of mitochondrial germinating (negative control),
344 did not induce mitophagy (Figure 11B). To be noted, the mitophapy became most
345 prominent at 9 hours after irradiation of the cells (Figure S4). These results indicate that
346 the early-staged radiation-induced mitochondrial germination would be suppressed by
347 the subsequent mitophagy, and if the mitochondrial damage was aggravated at higher
348 dose radiation, the mitochondrial biogenesis was then diminished in the late-stage of
349 the cell process.

350 **DISCUSSION**

351 Mitochondria as the cell energy factory play a vital role in cell homeostasis(Lill and
352 Freibert, 2020). In response to external stimuli, mitochondrial biogenesis can be elicited
353 in order to provide the cells with extra energy(Barros and McStay, 2019). Previously, many
354 studies had reported that mitochondrial biogenesis could suppress apoptosis(Yu et al.,

355 2013), i.e., apoptosis is negatively correlated with mitochondrial biogenesis. Some
356 studies even claimed that apoptosis occurred because of the absence of mitochondrial
357 biogenesis(Martins et al., 2015). But this understanding is not accurate, because to the
358 best of our knowledge, mitochondrial biogenesis should be occurring as the early event
359 prior to apoptosis, though it might be reduced or diminished later during the process of
360 cell apoptosis. So, to explore the relationship between mitochondrial biogenesis and
361 apoptosis, it is important to scrutinize the whole cell process and examine the respective
362 bio-effects at different time points. Would mitochondrial biogenesis occur preceding
363 the apoptosis? And, if there would be mitochondrial biogenesis occurring as the early
364 event of the apoptosis, how would it change with time? With these questions and
365 considerations, we thus initiated this research, and applied ionizing radiation as the tool
366 to induce both mitochondrial biogenesis and apoptosis in the cells, to explore the time-
367 dependent relationship between mitochondrial biogenesis and apoptosis. As a result, we
368 have thus achieved the following results with some new findings and elaborated
369 understandings.

370 Firstly, we have constructed the dual fluorescence report system that can be
371 effectively used for mitochondrial biogenesis study. To probe the changes taking place
372 in mitochondria, we have especially developed the approach using mitochondrial-
373 tagged recombinant fluorescent proteins. To the best of our knowledge, it is actually the
374 first time to apply the dual fluorescence ratio approach to study the biological effects
375 of mitochondria. According to the in situ and real-time observation of fluorescence in
376 the cell workstation and the high-throughput analysis of fluorescence ratio through
377 high-content quantitative analysis system, we have thus developed a new method of
378 using dual fluorescent reporter system for the the study of mitochondrial biogenesis,

379 which has been proved to be quite effective and reliable. As we know, the fluorescent
380 protein reporting system has the advantages of real-time, convenient, fast, and non-
381 destructive(Betzig et al., 2006). Besides, it has also an advantage in the study of
382 subcellular organ localization and protein stress regulation(Llopis et al., 1998).
383 Previously, people often used fluorescent dye probes for studying effect involved with
384 mitochondria. For example, Mukhopadhyay et al. used Annexin V and Sytox Green and
385 MitoSOX Red fluorescent probes to study the detection of apoptosis and mitochondrial
386 superoxide so as to establish the method for detecting living cells by laser confocal
387 scanning microscopy and flow cytometry (Mukhopadhyay et al., 2007). But the
388 disadvantages of fluorescent dyes are the toxicity to cells, as well as the light quenching
389 under long-period real-time observation. Compared to fluorescent dyes, fluorescent
390 proteins are more stable and have minimal toxicity and can generate visible
391 fluorescence in vivo (Westermann and Neupert, 2000). Actually, GFP reporter protein
392 is now commonly used to detect mitochondrial changes(Hanson et al., 2004; Mahajan
393 et al., 1998). In this work, in particular, we have constructed the dual fluorescence
394 reporting system based on fluorescence proteins for monitoring the mitochondrial
395 biogenesis process. We have also verified the effectiveness of this system designed for
396 monitoring mitochondrial biogenesis. For this purpose, we apply AICAR to activate
397 mitochondrial biogenesis as the positive control (Komen and Thorburn, 2014), as
398 AICAR is an activator of AMP-activated protein kinase (AMPK) that can permeate cell
399 membranes(Rai et al., 2015). AMPK (AMP activated protein kinase) is an activator of
400 mitochondrial biogenesis and key regulator of energy homeostasis caused by external

401 factors (Kim et al., 2016). The main function is to phosphorylate PGC-1α protein, or
402 affect the transduction of SIRT1 signaling pathway(Mihaylova and Shaw, 2011). Our
403 result clearly shows that AICAR indeed induced the up-regulation of key protein levels
404 of mitochondrial biogenesis. The prominent merit of such a dual fluorescent protein
405 reporter system is that it is not only suitable for the real-time in situ observation for a
406 long time, but also facilitates the precise fluorescence evaluation with the reference
407 fluorescent protein for intensity normalization, so that the interference from
408 background signal noise can be best avoided. Therefore, by analyzing the ratio of the
409 fluorescence intensity of mitochondrial DNA to that of nuclear DNA expression, the
410 early event of mitochondrial biogenesis under irradiation condition can be readily
411 observed and evaluated, and with this approach we can thus sensitively track the early
412 process that which would eventually lead to the late event of apoptosis.

413 Secondly, with the as-constructed dual fluorescence report system, we have
414 observed the radiation-induced mitochondrial biogenesis together with the apoptosis.
415 Ionizing radiation has been used for cancer therapy for they can directly or indirectly
416 cause DNA damage and kill the cancer cells(Spitz et al., 2004). With DNA damage
417 in the nucleus, cells may undergo cell cycle arrest required for repairing the damage or
418 cell death including apoptosis(Bernstein et al., 2002). In parallel, mitochondria is also
419 considered to be involved in the radiation induced effects, where more reactive oxygen
420 species (ROS) would be produced which may affect the cells profoundly. Actually, it
421 has been well documented that exposure of cells to ionizing radiation could activate
422 ROS to produce oxidases, regulate antioxidants, and alter metabolic activity in response

423 to oxidative damage(Azzam et al., 2012). In both the nucleic or mitochondrial processes,
424 more ATP is required to elicit mitochondria biogenesis either directly or
425 indirectly(Kulms et al., 2002; Srinivas et al., 2019). So, it is not surprising that
426 mitochondria biogenesis could take place as one of the consequences of radiation-
427 induced bio-effects (Galluzzi and Kroemer, 2008). But interestingly, in our fluorescence
428 measurements, we found that the fluorescence ratio increased and reached the
429 maximum at 6 h after irradiation, but afterwards the fluorescence ratio decreased
430 gradually. According to our established mitochondrial fluorescence report system, this
431 suggests that in the early stage, mitochondrial biogenesis was indeed initiated and
432 enhanced. In this process of mitochondrial biogenesis, mitochondrial DNA and
433 mitochondrial mass were maintained to keep the cell homeostasis and
434 metabolism(Huangyang et al., 2020). But in the late stage of the radiation effect, the
435 fluorescence ratio decreased, showing that the function of mitochondrial biogenesis
436 gradually diminished. We can also understand this change by relating it to the ROS
437 elevation. There was increase of ROS caused by radiation, which continuously
438 increased the oxidative stress and damaged the mtDNA and the mitochondrial integrity.
439 For the role of ROS, it is generally accepted that normal range of ROS may induce
440 stress response by changing the expression of related nuclear genes, and certain level
441 of ROS can save cells by maintaining energy metabolism (Srinivas et al., 2019); but
442 when the ROS level exceeds the tolerant threshold, ROS can then induce the transition
443 of mitochondrial membrane permeability, leading to the activation of the caspase
444 pathway and promoting cell apoptosis. In our experiment, we detected the increase of

445 ROS level in cytoplasm and mitochondria, the increase of calcium ion level in
446 cytoplasm and mitochondria, the decrease of ATP level and mitochondrial membrane
447 potential, the decrease of mitochondrial DNA copy number and mitochondrial citrate
448 synthase activity. All these results are consistent with each other. Also, given the
449 increase of radiation dose, we detected the related caspase-related proteins and found
450 that the increase of pro-apoptotic proteins such as cytochrome c. Release of cytochrome
451 c is an indicator for the apoptosis, in which the oxidative stress would damage mtDNA
452 and other components of the cells(Lee and Wei, 2005). Here, we especially notified that
453 the mitochondrial fluorescence intensity change rates were quite different after the cell
454 exposure to the radiation. The larger the irradiation dose, the higher the fluorescence
455 ratio reduction rate. All these observations are actually the typical features for the
456 radiation-induced apoptotic process.

457 Thirdly, our new observation has revealed the more subtle but very important
458 relationship which had largely been substantially or largely ignored by previous studies.
459 We noticed that in the beginning of the process, the mitochondrial biogenesis was
460 actually positively rather negatively associated with the apoptotic stress, and the trend
461 of fluorescence change was consistent with the number of apoptotic cells. This is
462 actually contrary to the conventional view on the relationship between mitochondrial
463 biogenesis and apoptosis. In the past, there were few reports concerning the dynamic
464 process of mitochondrial biogenesis, and the mainstream opinion or understanding on
465 the relationship between mitochondrial biogenesis and apoptosis was that these two
466 processes normally appear to be antagonistic. For example, many studies showed that

467 the apoptosis occurred simultaneously with the suppression, or, that apoptosis took
468 place with even missing the observation of mitochondrial biogenesis (Lin et al., 2020;
469 Martins et al., 2015; Vayssiere et al., 1994; Zhang et al., 2017). This is actually not true
470 or accurate, because mitochondrial biogenesis as an earlier event did occur preceding
471 the apoptosis, as we have clearly demonstrated in this study.

472 The reason for this misleading of understanding is largely due to the ignorance of
473 the investigation of the dynamic process of the cells. Generally, people tend to choose
474 just several time check points for inspecting the apoptosis and mitochondrial biogenesis.
475 But which time check points are most suitable for the correct evaluation? What cautions
476 should be taken to avoid the wrong evaluation when especially concerning the
477 relationship between the processes in the involvement? To solve this, we actually need
478 to establish more precise method to study the cellular effect in its dynamic process, and
479 so to scrutinize the processes of both mitochondrial biogenesis and apoptosis in their
480 logical time sequence. This is also one of the main purposes of this study. It is
481 understandable why people had not focused on the study of processes, as we realized
482 that there had been lack of tool/method for the monitoring the whole process regarding
483 the mitochondrial changes in situ and in a nondestructive way. For example, the
484 traditional methods include using real-time quantitative PCR to detect the copy number
485 of mitochondrial DNA, or using Western blot assay to identify the changes of marker
486 protein level of mitochondrial biogenesis. These methods cannot achieve in-situ and
487 real-time observation in living cells. On the contrary, the fluorescence protein method
488 can be used to observe the mitochondrial biogenesis in real time as especially useful for

489 studying the early events prior to apoptosis. Therefore, in this work, we for the first
490 time attempted to construct the fluorescent reporting system which could let us to track
491 the change of mitochondrial biogenesis. Based on the fluorescence signal, the dual
492 fluorescence ratio can help us to predict the radiation effects or the cell fate according
493 to the fluorescence change of these irradiated cells.

494 In particular, from the fluorescence data obtained from Figure 3C, we can calculate
495 the fluorescence ratios, and so we can retrieve the MFI ratios in each irradiation dose
496 group (0 Gy, 1 Gy, 2 Gy, 4 Gy) at an early time, as shown in Figures 12 A-B. Strikingly,
497 this result is consistent with the cells in the apoptotic state at 24 h (Figure 4E). In the
498 late stage (24 hours), the fluorescence ratio becomes smaller as the irradiation dose
499 increases. It is understandable because the apoptosis is actually dependent on the early
500 biochemical events in the cells(Holler et al., 2000). In this way, we may therefore infer
501 or predict the late apoptotic state of cells by observing the early-staged changes in terms
502 of mitochondrial fluorescence ratio. On the other hand, it is also seen that this
503 fluorescence ratio was significantly reduced after 24 h (Figure 12C), which is not
504 concomitant with the apoptosis at 24 h (Figure 4E). This suggests again that it is very
505 critical to evaluate both the processes by choosing the right time check points.

506 Finally, we have also tried to understand the mechanism for the mitochondrial
507 biogenesis related to the radiation-induced apoptosis. Generally, it is believed that the
508 biogenesis of mitochondria is a very complex biological process, which can maintain
509 the cell homeostasis by controlling the self-renewal of subcellular organelles and
510 maintaining mitochondrial DNA (Scarpulla, 2008). The initiation of mitochondrial

511 biogenesis is normally triggered by the reception of energy demand signals caused by
512 external stress (Popov, 2020), while at the same time, mitochondrial biogenesis itself is
513 a protection way for cell's self-renewal. Since it is well-known that ionizing radiation
514 is an effective way to stimulate the cell mitochondrial biogenesis, we thus employed
515 the tool of ionizing radiation to treat the cells. As a result, we have successfully proved
516 that some marker proteins of mitochondrial biogenesis are involved in the biological
517 effects of radiation. We have found that the protein expression levels of nuclear
518 respiratory factor1 (NRF1), peroxisome proliferative activated receptor, gamma,
519 coactivator 1 alpha (PGC-1α), transcription factor A, mitochondrial (TFAM) increased
520 with radiation dose. NRF1 is a transcription factor with a vital role in mitochondrial
521 functional genes(Virbasius et al., 1993). As a transcription coactivator, PGC-1α is a
522 central regulator of mitochondrial biogenesis and energy metabolism, and has become
523 a hot target for cancer treatment because of its relationship with cell death and oxidative
524 metabolism(Wang et al., 2019) (Bost and Kaminski, 2019) (Wu et al., 1999). TFAM is
525 a key activator of mitochondrial (mt) DNA transcription. mtDNA is reported to be very
526 susceptible to oxidative stress(May-Panloup et al., 2005). With the confirmation of
527 these factors, we have thus also again unambiguously confirmed that this mitochondrial
528 biogenesis is indeed related to radiation-induced cell adaptation and apoptosis.

529 But how to explain the suppression or disappearance of mitochondrial biogenesis
530 for the higher dose of radiation observed in the late stage of the cell process which
531 corresponds to the apoptosis? In our experiments, we observed that mitochondrial
532 biogenesis increased in the early stage of the cell process, but with the increase of

533 radiation dose, the mitochondrial biogenesis decreased substantially in the late stage.
534 Firstly, we speculate that this change of mitochondrial biogenesis is related to DNA
535 repair ability, and with increased radiation damage, the DNA repair mechanism was
536 destroyed. It was previously reported that mitochondrial biogenesis can enhance DNA
537 repair ability, and mitochondrial biogenesis is closely related to DNA repair ability(Li
538 et al., 2020) (Fu et al., 2008). For example, it was reported that doxorubicin, a drug
539 which can induce DSBs of DNA as accompanied by mitochondrial biogenesis (Kluza
540 et al., 2004). Normally, there are two main repair pathways of DSBs in mammalian
541 cells: non homologous end joining (NHEJ) and homologous recombination mediated
542 repair (HR) (Löbrich and Jeggo, 2005). Mitochondrial biogenesis can promote DNA
543 repair by inducing chromatin changes in DSB and regulating the activity of DNA repair
544 factors, and this upstream factor has been found to be the silent information regulator
545 (SIRT) (Paredes and Chua, 2016). SIRT is a family of sirtuins that depend on NAD^+
546 lysine deacetylases, which may play an important role in mitochondrial biogenesis and
547 cell metabolism(Chalkiadaki and Guarente, 2015). On the other hand, DSB repair can
548 be achieved by NHEJ which can activate DNA-PK (Davis et al., 2014), while DNA-
549 PK can activate AMPK signal pathway, which is just closely related to mitochondrial
550 biogenesis (Park et al., 2017). In our experiment, we have indeed observed the change
551 of DNA repair as reflected by the change of 53BP1, and this change is just concomitant
552 with the mitochondrial biogenesis. Secondly, we also speculate that the mitochondrial
553 autophagy induced by radiation occurred, which subsequently cleared up the ROS-
554 damaged and dysfunctional mitochondria. According to the analysis of the mitophagy

555 result, we found that mitophagy increased with radiation dose at 9 hours after the cell
556 irradiation, although 24 hours after the irradiation, this process also diminished with the
557 death of the cells.

558 So, with the above findings and discussion of mechanisms, we can therefore
559 concisely describe the process of radiation affecting cells as schematically depicted in
560 Figure 13. After a certain dose of radiation, DNA damage occurs, and the cell cycle is
561 blocked in order to initiate the repair process. At the same time, radiation produces a
562 large amount of ROS in the cell and affects the homeostasis of the cell. To resist the
563 radiation stress or damage, mitochondria then start to provide more energy for DNA
564 repair and maintenance of cell metabolism and homeostasis, leading to mitochondrial
565 biogenesis. Next, with the continuous increase of ROS in cytoplasm and mitochondria,
566 the increase of calcium ions released to mediate the imbalance of mitochondrial energy
567 metabolism homeostasis, the decrease of ATP level and the decrease of citrate synthase
568 activity, the decrease of mitochondrial membrane potential which eventually led to the
569 release of Pro apoptotic protein cytochrome c and the activation of apoptotic caspase
570 pathway, the programmed cell death was elicited, with the diminishing of mitochondrial
571 biogenesis in the late stage of the cell process.

572

573 **CONCLUSION**

574 In this work, we have constructed a dual fluorescence reporting system, which
575 makes use of the intensity ratio of multiple fluorescence tags to observe the changes of
576 mitochondria in real time, and these changes are related to ionizing radiation-induced

mitochondrial biogenesis and apoptosis. We have also demonstrated that ionizing radiation can effectively cause mitochondrial biogenesis, so that it can be an efficient tool for the study of mitochondrial biogenesis. Particularly, for the exploration of the involved mechanisms, we have scrutinized the relationship between this mitochondrial biogenesis and apoptosis by considering the time sequence of occurrence. Our results have unambiguously proved that these two processes are not antagonistic if they are evaluated at right time points, but on the contrary, they may be positively correlated if we relate the mitochondrial biogenesis taking place at the early time to the apoptosis occurring at the late stage. Therefore, this work not only provides an effective method for directly observing the mitochondrial biogenesis process in living cells, but also demonstrates how to evaluate the biological effects correctly with right timing, with which we may be able to predict the cell fate such as apoptosis through the observation of the early event of cell process.

590 # STAR METHODS

591 ## RESOURCE AVAILABILITY

592 ### Lead Contact

593 Further information and requests for reagents may be directed to the lead contact, Qing
594 Huang (huangq@ipp.ac.cn).

595 ### Materials Availability

596 Reagents or materials used in this work may be requested from the Lead Contact by
597 signing a completed material transfer agreement.

598 ### Data and code availability

599 Original data generated by this study are available upon request.

600 ## EXPERIMENTAL MODEL AND SUBJECT DETAILS

601 ### Reagents

602 The *Escherichia coli* DH5a and DNA Ladder were purchased from Transgen (Beijing,
603 China). *Nhe*I, *Hind*III, *EcoR*I, *Not*I restriction enzymes, T4 DNA Ligase, and Q5 High-
604 Fidelity DNA Polymerase were purchased from NEB (MA, USA). Plasmid pEGFP-N1
605 was purchased from Clonetech Biotechnology (CA, USA). Plasmid pLVX-mCherry,
606 PUC57 were stored in our laboratory. Plasmids of psPAX2 (# 12260) and pMD.2G
607 (#12259) were purchased from Addgene. PCR purification and gel extraction kits were
608 obtained from Axygen (CA, USA). TRIzol™ reagent, Lipofectamine 2000 were
609 purchased from Invitrogen (CA, USA). Primescript II 1st strand cDNA Synthesis Kit,
610 RT-qPCR kit and Total genomic DNA extraction kit were purchased from TAKARA

611 (Dalian, China). G418 and Hoechst 33342 were purchased from Targetmol (Shanghai,
612 China). Citrate Synthase Assay Kit was purchased from Solarbio (Beijing, China).
613 Reactive oxygen species (ROS) probe (CellROX Green and MitoSOX Red) was
614 purchased from Invitrogen. JC-1 dye was purchased from Beyotime. 5-
615 Aminoimidazole-4-carboxamide ribotide (AICAR) was purchase from Selleck (MA,
616 USA). The antibodies of PGC-1α, NRF1, TFAM, Mfn1, BAX, Bcl-2, CytoC, Caspase-
617 3, Cleaved Caspase-9, PARP, γH2AX(S139), GFP, p-AMPK were purchased from
618 Bimake (MA, USA), 53BP1, anti-β-Actin antibody was purchased from CST (MA,
619 USA). Alexa Fluor® 488 Goat Anti-Mouse (IgG) secondary antibody, Alexa Fluor®
620 647 Goat Anti-Rat (IgG) secondary antibody were purchased from Invitrogen (CA,
621 USA).

622 **METHOD DETAILS**

623 **Creation of stably transfected cell lines**

624 **Generation of plasmids.** Firstly, the pEGFP-N1-COX8 expression plasmid was
625 constructed. Briefly, the DNA sequence of cytochrome c oxidase 8A subunit was found
626 from Genbank (NM_004074.2) (Hendrickson et al., 2010). Then, two complementary
627 oligonucleotide strands were obtained by amplification using PCR, and the restriction
628 sites of the *Nhe*I and *Hind*III were added at both ends. The sequences of oligonucleotide
629 strands were listed in Table S1 (Supporting information). The DNA sequence (COX8A)
630 was ligated on the PUC57 plasmid. Then, the appropriate oligonucleotides were
631 annealed and ligated into pEGFP-N1 cloning cut with *Nhe*I and *Hind*III. After
632 incubation overnight at 37°C, the target plasmids were extracted from the bacterial fluid
633 using the EndoFree Maxi Plasmid kit.

634 Secondly, the PLVX-mCherry-Actin expression plasmid was constructed. Total
635 RNA was extracted from HeLa cells by Trizol reagent and served as the template for
636 cDNA synthesis, and then it was reversely transcripted using Primescript II 1st strand
637 cDNA synthesis kit. The primers were designed according to the sequence of actin
638 (Genbank no. NM_10277): *EcoR*I tailed forward (5′-
639 gtcGAATTCatggatgatgatatcgccgcgc-3′) and *Not*I tailed reverse (5′-
640 TATGCGGCCGCctagaagcatttgcggtggac-3′) primers which are named as Fw-actin-
641 EcoRI and Rv-actin-NotI, respectively. The length of the amplified product was 1128
642 bp. The PCR product was separated by electrophoresis, and the target fragment was

643 recovered after gel cutting and purification. The target gene fragment (actin) and the
644 expression vector (pLVX-mCherry) with the same restriction site (*EcoR*I and *Not*I)
645 were digested by restriction enzymes respectively, and then ligated with T4 ligase and
646 transformed into *E. coli* DH5a for plasmid amplification.

647 **Production of lentiviral supernatant and transduction of COX8-EGFP-mCherry-**
648 **ACTIN-HeLa.** Briefly, positive monoclonal cells (COX8-EGFP-HeLa cells) were
649 constructed. When HeLa cells grew to the concentration of 80% in complete medium,
650 they were then transfected with pEGFP-COX8 plasmid with lipofectamine 2000. After
651 24-48 h of transfection, G418 was added to screen positive monoclonal cells.

652 The lentiviral supernatant was prepared according to the protocol provided by
653 addgene (http://www.addgene.org/tools/protocols/plko/#A). When the confluence of
654 HEK293T cells cells in the 6-well plate reached 80%, Lipofectamine 2000 was used to
655 transfect the pLVX-mCherry-ACTIN plasmid and the viral packaging helper plasmid
656 psPAX2, pMD.2G into the cells. After incubation for 8h, the medium was replaced with
657 the fresh medium containing serum, and the supernatant was collected 24 hours and 48
658 hours later. The virus supernatant was filtered through a 0.45 μm pore so as to infect
659 COX8-EGFP-HeLa cells. Next, the COX8-EGFP-HeLa cells were cultured in a 6-well
660 plate to 70% confluence, then the medium was removed, and the virus supernatant was
661 mixed with fresh medium containing 8 μg/ml polybrene in equal proportions and added
662 to the culture plate. The fresh medium was replaced after 24 hours and the medium
663 containing 1 μg/ml puromycin was changed at 48 hours to start screening to obtain

664 stable cell lines.

665 **Cell Culture, Synchronization and Gamma irradiation**

666 HeLa, HEK-293T cell lines were purchased from American Type Cultures
667 Collection (ATCC, Manassas, VA). The HeLa and HEK-293T cells were cultured in
668 Dulbecco's modified Eagle's medium (DMEM, HyClone) containing 10% fetal bovine
669 serum (FBS, Gibco BRL). All cells were maintained at 37 °C in 5% CO2.

670 The cell cycle synchronization method was detailed in the previous work
671 (Rodríguez-Martínez et al., 2020). The cells were incubated with thymidine (2.5 mM)
672 for 18 hours, washed once with PBS buffer and replaced with fresh medium for 14
673 hours, and then 2.5 mM thymidine was added again to the cells which were then
674 incubated for 18 hours. The efficiency of synchronization was tested by flow cytometry
675 using cell cycle analysis kit (Multisciences).

676 HeLa cells were irradiated by gamma-ray provided by a Biobeam Cs137 irradiator
677 (cat no. GM 2000; Gamma-Service Medical, Leipzig, Germany), with the doses of 1,
678 2, and 4 Gy at the dose rate of 3.37 Gy/ min. In the control group, the cells were taken
679 out of the incubator without irradiation.

680 **Cell viability, LDH measurements and colony-formation assays**

681 Cell viability was measured with CCK-8 assay kit (Dojindo, Japan). Briefly, 24 h
682 prior to irradiation treatment, ca. 6000 cells were plated in 96-well plates in a final
683 volume of 100 μl, and then cultured for 24 h. And after adding the CCK-8 solution, the
684 plate was incubated for another 1 h. The optical density was measured at 450 nm using
685 a microplate reader (SpectraMax M5, Molecular Devices, USA). The amount of LDH
686 released into the medium was assayed using the LDH-Cytotoxicity Assay Kit II
687 (Dojindo, Japan) according to the manufacturer's instructions. For the colony formation
688 assay, 500 cells were seeded in 6-well plate. After being irradiated, the cells were
689 cultured at 37℃ for about 2 weeks. After carefully washing twice with PBS, 4%
690 paraformaldehyde was added to fix the cells. The the cells were then stained with crystal
691 violet solution and evaluated.

692 **Analysis of Cytosolic ROS and Mitochondrial ROS**

693 Cytosolic ROS and mitochondrial ROS were detected by CellROX Green and
694 MitoSOX Red probes, respectively. The HeLa cells were plated in corning 96-well plate
695 at a density of 8000 cells/ well, cultivated overnight. At 6 h after irradiation, cells were
696 incubated with 5 μM CellROX Green probe or 5 mM MitoSOX Red probe staining
697 solution for 30 min. Then, the HeLa cells were washed with HBSS buffer thrice and
698 incubated with 2 μg/ml Hoechst 33342 for 10 min. Fluorescent signals were analyzed
699 by Thermo CX5 HCS fluorescence microscopy.

700 **Analysis of mitochondrial membrane potential**

701 Mitochondrial membrane potential ($\Delta\Psi_m$) was measured using the JC-1 probe with

702 the mitochondrial membrane potential assay kit (Beyotime, China) according to the
703 manufacturer's instructions. Briefly, the HeLa cells were seeded in 96 well plates with
704 8000 cells per well and cultured overnight at 37 °C. After 12 hours of irradiation, the
705 HeLa cells were incubated with 1 mg/ml JC-1 and 2 μg/ml Hoechst 33342 in dark for
706 20 minutes, washed with HBSS buffer for 3 times, and then photographed with Thermo
707 CX5 HCS fluorescence microscope or quantitatively analyzed with flow cytometry.
708 The monomer fluorescence (green) of JC-1 was observed at emission Em=521 nm with
709 excitation Ex=485 nm, and the aggregated fluorescence (red) of JC-1 was observed at
710 Em=607 nm with Ex=560 nm.

711 **Annexin V-FITC/PI staining and cell cycle analysis**

712 The HeLa cells were seeded at 2×10^5 cell /well in 6-well plates and irradiation
713 with gamma-ray. After 24 h, the cells were fixed with cold ethanol and then stained with
714 propidium iodide according to kit manuscript (MultiSciences). The cells (about 20,000)
715 were analyzed by flow cytometry (Beckman CytoFLEX, USA). The total cells were
716 washed once and resuspended in Annexin V binding buffer, and then stained with 5 μl
717 Annexin V and 5μl PI (Roche, Germany) for 20 min and analyzed with Beckman
718 CytoFLEX flow cytometry. Ten thousand events were collected for each sample.

719 **Evaluation of citrate synthase (CS) activity**

720 Citrate synthase (CS) activity was determined using a citrate synthase activity
721 assay kit (Solarbio, China). According to the instruction of the kit, the protein

722 concentration was determined after cell lysis. Then, 7 μL protein was mixed with other
723 reagents in the kit and put into a slit quartz cuvette. The initial absorbance A1 was
724 recorded at 412 nm for 10 seconds. The whole quartz cuvette was then put into a 37 °C
725 water bath. After 2 minutes of reaction, it was taken out, and the absorbance A2 was
726 recorded at 412 nm, so the OD value was calculated Δ A=A2-A1. CS enzyme activity
727 was calculated according to the formula provided with the assay kit.

728 **Intracellular Ca^{2+} Measurement**

729 The HeLa cells were loaded with the Ca^{2+} indicator Fluo-4 AM probe to assess the
730 intracellular calcium signaling after cell irradiation at 6 h. Rhod-2 AM was used to
731 monitor the changes in mitochondrial calcium concentrations. Fluorescent signals were
732 analyzed by Thermo CX5 HCS fluorescence microscopy.

733 **Mito-Keima mitophagy analysis**

734 The HeLa cells were transfected with the mKeima-Red-Mito-7 plasmid using
735 Lipo2000. After irradiation with gamma-ray, the nuclei were stained with Hoechst
736 33342. The fluorescence was measured with Thermo CX5 HCS fluorescence
737 microscope and the ratio of fluorescence at 560 nm over fluorescence at 485 nm Keima
738 fluorescence was calculated to reflect the level of mitophagy.

739 **Determination of ATP levels**

740 Intracellular ATP measured using a luciferin/luciferase assay kit (Invitrogen,
741 USA). Cells were cultured in a black 96 well plates at density of 1×10^5 cells per well.
742 After irradiated with gamma-ray, the cells were washed with HBSS and then lysed

743 according to the manufacturer's instructions. Luminescence (which is proportional to
744 the amount of ATP) was measured with SpectraMax M5 microplate reader.

745 **Measurement of mitochondrial to nuclear DNA ratio (mtDNA/ nDNA)**

746 Total genomic DNA of HeLa cells was extracted after irradiation using Total
747 genomic DNA extract kit (TAKARA, China). Human nuclear GAPDH gene (forward:
748 5′- CAGAACATCATCCCTGCCTCTAC-3′; reverse: 5′-
749 AAGGGTTGTAGTAGCCCGTAG-3′) and the mtDNA ND1 gene (forward: 5′-
750 TTCTAATCGCAATGGCATTCCT-3′; reverse: 5′-
751 AAGGGTTGTAGTAGCCCGTAG-3′), as well as a primer were used to detect the
752 mtDNA copy number. The real-time quantitative PCR analysis was performed using
753 SYBR Premix Ex Taq II (TAKARA, China) on LightCycler 480 PCR System (Roche,
754 Germany). The calculations were analyzed with $2^{-\Delta\Delta Ct}$ method.

755 **Analysis of mean fluorescence intensity（MFI）of dual fluorescent protein**

756 MFI of the dual fluorescent protein was analyzed using a flow cytometer. The cells
757 were treated with different radiation doses and collected at different time points, washed
758 with PBS buffer, then assessed by flow cytometry (Beckman CytoFLEX, USA). The
759 data were analyzed using Flow Jo software. The ratio of the MFI of EGFP to MFI of
760 mecherry was used for calculation and analysis. Each irradiated dose sample group was
761 analyzed for ca. 10,000 cells, and three measurements were repeated.

762 Furthermore, the High-Content Screening system Cell Insight CX5 HCS (Thermo

763 Fisher, Waltham, MA) was used for automatic photo quantitative analysis(Sun et al.,
764 2016). The dual-fluorescent protein HeLa cells were seeded in 96-well plates by
765 irradiated 1 Gy, 2 Gy, 4 Gy gamma-ray. The nuclei were stained with Hoechst 33342
766 (Targetmol). Fluorescence ratios of protein expression of mitochondrial expressed
767 COX8-EGFP and actin-mCherry were statistically analyzed by cellomics software
768 (Thermo Fisher, Waltham, MA).

769 **Laser scanning confocal fluorescence microscopy**

770 All the images were obtained using 488 nm and 561 nm lasers to excite cox8-
771 EGFP-actin-mCherry, while the 405 nm laser lines was used to excite DAPI. The
772 imaging was performed in line mode, the z-stack was over-sampled and photographed
773 at the height of 0.7 microns, and the image was acquired on the LEICA SP8 confocal
774 microscope system. The contrast and brightness of the image were adjusted by
775 Application Suite X (LEICA).

776 **Western blotting analysis and immunofluorescence staining assay**

777 Total proteins were extracted from cells using RIPA lysis buffer with a protease
778 inhibitor cocktail (Roche, Germany). The proteins were quantified using Thermo
779 Scientific Pierce BCA Protein Assay. The protein level of Bax, Bcl-2, caspase-3,
780 cleaved caspase-9, Cytoc, p-AMPK, PARP, TFAM, Mfn1, PGC-1α, GFP and loading
781 control β-Actin were determined by Western blotting assay.

782 For immunofluorescence staining, HeLa cells were grown on chamber slides. After

783 γ-ray irradiation or mock irradiation, they were fixed with cold methanol for 10 minutes
784 and permeated with 0.5% Triton X-100 in PBS for 20 minutes. After blocking for 1
785 hour, the cells were incubated with the primary antibody overnight and then incubated
786 with the fluorescently labeled secondary antibody for 1 hour at 37°C. Samples
787 investigated by laser confocal microscopy (LEICA). Image auto-quantification and co-
788 localized foci were recognized by CellProfiler version 4
789 (www.cellprofiler.org)(McQuin et al., 2018).

790 **Statistical analysis**

791 Data were presented as mean ± standard deviation (SD). Statistical significance was
792 assessed by one-way or two-way ANOVA via GraphPad Prism software (Prism version
793 9, San Diego, CA, USA). *P*-Value < 0.05 was considered as statistically significant.

794

795

ACKNOWLEDGEMENTS

This work was supported by the National Natural Science Foundation of China (grants No. 11635013 and No. 11775272) and Special Repair and Purchase Fund for Central-level scientific institutions (No. Y79XG13361).

AUTHOR CONTRIBUTIONS

QH conceived the idea and supervised the research. CS and QH designed and performed the experiments, analyzed and interpreted data, performed statistical analysis, and wrote the manuscript. XZ, YM, PW and QZ provided technical assistance in the experiments. All authors read and approved the final manuscript.

DISCLOSURES

The authors declare that they have no competing interests.

809 **References:**

810

811 Azzam, E.I., Jay-Gerin, J.-P., and Pain, D. (2012). Ionizing radiation-induced metabolic oxidative
812 stress and prolonged cell injury. Cancer Lett *327*, 48–60.

813 Barros, M.H., and McStay, G.P. (2019). Modular Biogenesis of Mitochondrial Respiratory
814 Complexes. Mitochondrion *50*, 94–114.

815 Bernstein, C., Bernstein, H., Payne, C.M., and Garewal, H. (2002). DNA repair/pro-apoptotic
816 dual-role proteins in five major DNA repair pathways: fail-safe protection against carcinogenesis.
817 Mutat Res Rev Mutat Res *511*, 145–178.

818 Betzig, E., Patterson, G.H., Sougrat, R., Lindwasser, O.W., Olenych, S., Bonifacino, J.S.,
819 Davidson, M.W., Lippincott-Schwartz, J., and Hess, H.F. (2006). Imaging Intracellular
820 Fluorescent Proteins at Nanometer Resolution. Science *313*, 1642–1645.

821 Bost, F., and Kaminski, L. (2019). The metabolic modulator PGC-1α in cancer. Am J Cancer Res
822 *9*, 198–211.

823 Burke, P.J. (2017). Mitochondria, Bioenergetics and Apoptosis in Cancer. Trends Cancer *3*, 857–
824 870.

825 Cao, C., Yu, H., Wu, F., Qi, H., and He, J. (2017). Antibiotic anisomycin induces cell cycle arrest
826 and apoptosis through inhibiting mitochondrial biogenesis in osteosarcoma. J Bioenerg Biomembr
827 *49*, 437–443.

828 Chalkiadaki, A., and Guarente, L. (2015). The multifaceted functions of sirtuins in cancer. Nat
829 Rev Cancer *15*, 608–624.

830 Dam, A.D., Mitchell, A.S., and Quadrilatero, J. (2013). Induction of mitochondrial biogenesis
831 protects against caspase-dependent and caspase-independent apoptosis in L6 myoblasts.
832 Biochimica Et Biophysica Acta Bba - Mol Cell Res *1833*, 3426–3435.

833 Das, S., Joshi, M.B., Parashiva, G.K., and Rao, S.B.S. (2020). Stimulation of cytoprotective
834 autophagy and components of mitochondrial biogenesis / proteostasis in response to ionizing
835 radiation as a credible pro-survival strategy. Free Radical Bio Med.

836 Davis, A.J., Chen, B.P.C., and Chen, D.J. (2014). DNA-PK: A dynamic enzyme in a versatile
837 DSB repair pathway. Dna Repair *17*, 21–29.

838 Fanibunda, S.E., Deb, S., Maniyadath, B., Tiwari, P., Ghai, U., Gupta, S., Figueiredo, D.,
839 Weisstaub, N., Gingrich, J.A., Vaidya, A.D.B., et al. (2019). Serotonin regulates mitochondrial
840 biogenesis and function in rodent cortical neurons via the 5-HT2A receptor and SIRT1–PGC-1α
841 axis. Proc National Acad Sci *116*, 201821332.

842 Fu, X., Wan, S., Lyu, Y.L., Liu, L.F., and Qi, H. (2008). Etoposide Induces ATM-Dependent
843 Mitochondrial Biogenesis through AMPK Activation. Plos One *3*, e2009.

844 Galluzzi, L., and Kroemer, G. (2008). Necroptosis: a specialized pathway of programmed
845 necrosis. Cell *135*, 1161–1163.

846 Haggie, P.M., and Verkman, A.S. (2002). Diffusion of Tricarboxylic Acid Cycle Enzymes in the
847 Mitochondrial Matrixin Vivo: EVIDENCE FOR RESTRICTED MOBILITY OF A
848 MULTIENZYME COMPLEX. J Biol Chem *277*, 40782–40788.

849 Hanson, G.T., Aggeler, R., Oglesbee, D., Cannon, M., Capaldi, R.A., Tsien, R.Y., and Remington,
850 S.J. (2004). Investigating Mitochondrial Redox Potential with Redox-sensitive Green Fluorescent
851 Protein Indicators. J Biol Chem *279*, 13044–13053.

852 Holler, N., Zaru, R., Micheau, O., Thome, M., Attinger, A., Valitutti, S., Bodmer, J.-L., Schneider,
853 P., Seed, B., and Tschopp, J. (2000). Fas triggers an alternative, caspase-8–independent cell death
854 pathway using the kinase RIP as effector molecule. Nat Immunol *1*, 489–495.

855 Huangyang, P., Li, F., Lee, P., Nissim, I., Weljie, A.M., Mancuso, A., Li, B., Keith, B., Yoon,
856 S.S., and Simon, M.C. (2020). Fructose-1,6-Bisphosphatase 2 Inhibits Sarcoma Progression by
857 Restraining Mitochondrial Biogenesis. Cell Metab *31*, 1032.

858 Jadhav, U., and Shivdasani, R.A. (2019). Dissecting Cell Lineages: From Microscope to
859 Kaleidoscope. Cell *176*, 949–951.

860 Katajisto, P., Döhla, J., Chaffer, C.L., Pentinmikko, N., Marjanovic, N., Iqbal, S., Zoncu, R.,
861 Chen, W., Weinberg, R.A., and Sabatini, D.M. (2015). Stem cells. Asymmetric apportioning of
862 aged mitochondria between daughter cells is required for stemness. Sci New York N Y *348*, 340–
863 343.

864 Kim, J., Yang, G., Kim, Y., Kim, J., and Ha, J. (2016). AMPK activators: mechanisms of action
865 and physiological activities. Exp Mol Medicine *48*, e224–e224.

866 Kluza, J., Marchetti, P., Gallego, M.-A., Lancel, S., Fournier, C., Loyens, A., Beauvillain, J.-C.,
867 and Bailly, C. (2004). Mitochondrial proliferation during apoptosis induced by anticancer agents:
868 effects of doxorubicin and mitoxantrone on cancer and cardiac cells. Oncogene *23*, 7018–7030.

869 Komen, J.C., and Thorburn, D.R. (2014). Turn up the power – pharmacological activation of
870 mitochondrial biogenesis in mouse models. Brit J Pharmacol *171*, 1818–1836.

871 Kulms, D., Zeise, E., Pöppelmann, B., and Schwarz, T. (2002). DNA damage, death receptor
872 activation and reactive oxygen species contribute to ultraviolet radiation-induced apoptosis in an
873 essential and independent way. Oncogene *21*, 5844–5851.

874 Leach, J.K., Tuyle, G.V., Lin, P.S., Schmidt-Ullrich, R., and Mikkelsen, R.B. (2001). Ionizing
875 radiation-induced, mitochondria-dependent generation of reactive oxygen/nitrogen. Cancer Res
876 *61*, 3894–3901.

877 Lee, H.-C., and Wei, Y.-H. (2005). Mitochondrial biogenesis and mitochondrial DNA
878 maintenance of mammalian cells under oxidative stress. Int J Biochem Cell Biology *37*, 822–834.

879 Li, S., Shi, B., Liu, X., and An, H.-X. (2020). Acetylation and Deacetylation of DNA Repair
880 Proteins in Cancers. Frontiers Oncol *10*, 573502.

881 Lill, R., and Freibert, S.-A. (2020). Mechanisms of Mitochondrial Iron-Sulfur Protein Biogenesis.
882 Annu Rev Biochem *89*, 471–499.

883 Lin, W.T., Nithiyanantham, S., Hsieh, D.J., Chen, R., Day, C., Liao, J.Y., Kuo, C., Mahalakshmi,
884 B., Kuo, W., and Huang, C. (2020). Bioactive peptides attenuate cardiac apoptosis in
885 spontaneously hypertensive rat hearts through activation of autophagy and mitochondrial
886 biogenesis pathway. Environ Toxicol *35*, 804–810.

887 Llopis, J., McCaffery, J.M., Miyawaki, A., Farquhar, M.G., and Tsien, R.Y. (1998). Measurement
888 of cytosolic, mitochondrial, and Golgi pH in single living cells with green fluorescent proteins.
889 Proc National Acad Sci *95*, 6803–6808.

890 Löbrich, M., and Jeggo, P.A. (2005). Harmonising the response to DSBs: a new string in the ATM
891 bow. Dna Repair *4*, 749–759.

892 Mahajan, N.P., Linder, K., Berry, G., Gordon, G.W., Heim, R., and Herman, B. (1998). Bcl-2 and
893 Bax interactions in mitochondria probed with green fluorescent protein and fluorescence
894 resonance energy transfer. Nat Biotechnol *16*, 547–552.

895 Martins, L.A.M., Vieira, M.Q., Ilha, M., Vasconcelos, M. de, Biehl, H.B., Lima, D.B., Schein, V.,
896 Barbé-Tuana, F., Borojevic, R., and Guma, F.C.R. (2015). The Interplay Between Apoptosis,
897 Mitophagy and Mitochondrial Biogenesis Induced by Resveratrol Can Determine Activated
898 Hepatic Stellate Cells Death or Survival. Cell Biochem Biophys *71*, 657–672.

899 May-Panloup, P., Vignon, X., Chrétien, M.-F., Heyman, Y., Tamassia, M., Malthièry, Y., and
900 Reynier, P. (2005). Increase of mitochondrial DNA content and transcripts in early bovine
901 embryogenesis associated with upregulation of mtTFA and NRF1 transcription factors. Reprod
902 Biol Endocrin *3*, 65.

903 McQuin, C., Goodman, A., Chernyshev, V., Kamentsky, L., Cimini, B.A., Karhohs, K.W., Doan,
904 M., Ding, L., Rafelski, S.M., Thirstrup, D., et al. (2018). CellProfiler 3.0: Next-generation image
905 processing for biology. Plos Biol *16*, e2005970.

906 Melentijevic, I., Toth, M.L., Arnold, M.L., Guasp, R.J., Harinath, G., Nguyen, K.C., Taub, D.,
907 Parker, J.A., Neri, C., Gabel, C.V., et al. (2017). C. elegans neurons jettison protein aggregates
908 and mitochondria under neurotoxic stress. Nature *542*, 367–371.

909 Mihaylova, M.M., and Shaw, R.J. (2011). The AMPK signalling pathway coordinates cell growth,
910 autophagy and metabolism. Nat Cell Biol *13*, 1016–1023.

911 Miyashiro, T., and Goulian, M. (2007). Methods in Enzymology. Methods Enzymol *423*, 458–
912 475.

913 Montava-Garriga, L., and Ganley, I.G. (2019). Outstanding Questions in Mitophagy: What we Do
914 and Do Not Know. J Mol Biol *432*, 206–230.

915 Mukhopadhyay, P., Rajesh, M., Haskó, G., Hawkins, B.J., Madesh, M., and Pacher, P. (2007).
916 Simultaneous detection of apoptosis and mitochondrial superoxide production in live cells by flow
917 cytometry and confocal microscopy. Nat Protoc *2*, 2295–2301.

918 Newman, R.H., Fosbrink, M.D., and Zhang, J. (2011). Genetically encodable fluorescent
919 biosensors for tracking signaling dynamics in living cells. Chem Rev *111*, 3614–3666.

920 O'Driscoll, M., and Jeggo, P.A. (2006). The role of double-strand break repair — insights from
921 human genetics. Nat Rev Genet *7*, 45–54.

922 Paredes, S., and Chua, K.F. (2016). SIRT7 clears the way for DNA repair. Embo J *35*, 1483–1485.

923 Park, S.-J., Gavrilova, O., Brown, A.L., Soto, J.E., Bremner, S., Kim, J., Xu, X., Yang, S., Um, J.-
924 H., Koch, L.G., et al. (2017). DNA-PK Promotes the Mitochondrial, Metabolic, and Physical
925 Decline that Occurs During Aging. Cell Metab *25*, 1135-1146.e7.

926 Popov, L. (2020). Mitochondrial biogenesis: An update. J Cell Mol Med *24*, 4892–4899.

927 Rai, P.K., Russell, O.M., Lightowlers, R.N., and Turnbull, D.M. (2015). Potential compounds for
928 the treatment of mitochondrial disease. Brit Med Bull *116*, 5–18.

929 Rai, Y., Pathak, R., Kumari, N., Sah, D.K., Pandey, S., Kalra, N., Soni, R., Dwarakanath, B.S.,
930 and Bhatt, A.N. (2018). Mitochondrial biogenesis and metabolic hyperactivation limits the
931 application of MTT assay in the estimation of radiation induced growth inhibition. Sci Rep-Uk *8*,
932 1531.

933 Ruan, L., Zhou, C., Jin, E., Kucharavy, A., Zhang, Y., Wen, Z., Florens, L., and Li, R. (2017).
934 Cytosolic proteostasis through importing of misfolded proteins into mitochondria. Nature *543*,
935 443–446.

936 Scarpulla, R.C. (2008). Transcriptional Paradigms in Mammalian Mitochondrial Biogenesis and
937 Function. Physiol Rev *88*, 611–638.

938 Spitz, D.R., Azzam, E.I., Li, J.J., and Gius, D. (2004). Metabolic oxidation/reduction reactions and
939 cellular responses to ionizing radiation: A unifying concept in stress response biology. Cancer
940 Metast Rev *23*, 311–322.

941 Srinivas, U.S., Tan, B.W.Q., Vellayappan, B.A., and Jeyasekharan, A.D. (2019). ROS and the
942 DNA damage response in cancer. Redox Biol *25*, 101084.

943 Sun, J., Li, N., Oh, K.-S., Dutta, B., Vayttaden, S.J., Lin, B., Ebert, T.S., Nardo, D.D., Davis, J.,
944 Bagirzadeh, R., et al. (2016). Comprehensive RNAi-based screening of human and mouse TLR
945 pathways identifies species-specific preferences in signaling protein use. Sci Signal *9*, ra3–ra3.

946 Vayssiere, J.L., Petit, P.X., Risler, Y., and Mignotte, B. (1994). Commitment to apoptosis is
947 associated with changes in mitochondrial biogenesis and activity in cell lines conditionally
948 immortalized with simian virus 40. Proc National Acad Sci *91*, 11752–11756.

949 Virbasius, C.A., Virbasius, J.V., and Scarpulla, R.C. (1993). NRF-1, an activator involved in
950 nuclear-mitochondrial interactions, utilizes a new DNA-binding domain conserved in a family of
951 developmental regulators. Gene Dev *7*, 2431–2445.

952 Wang, Y., An, H., Liu, T., Qin, C., Sesaki, H., Guo, S., Radovick, S., Hussain, M., Maheshwari,
953 A., Wondisford, F.E., et al. (2019). Metformin Improves Mitochondrial Respiratory Activity
954 through Activation of AMPK. Cell Reports *29*, 1511-1523.e5.

955 Westermann, B., and Neupert, W. (2000). Mitochondria-targeted green fluorescent proteins:
956 convenient tools for the study of organelle biogenesis inSaccharomyces cerevisiae. Yeast *16*,
957 1421–1427.

958 Wu, Z., Puigserver, P., Andersson, U., Zhang, C., Adelmant, G., Mootha, V., Troy, A., Cinti, S.,
959 Lowell, B., Scarpulla, R.C., et al. (1999). Mechanisms Controlling Mitochondrial Biogenesis and
960 Respiration through the Thermogenic Coactivator PGC-1. Cell *98*, 115–124.

961 Yambire, K.F., Fernandez-Mosquera, L., Steinfeld, R., Mühle, C., Ikonen, E., Milosevic, I., and
962 Raimundo, N. (2019). Mitochondrial biogenesis is transcriptionally repressed in lysosomal lipid
963 storage diseases. Elife *8*, e39598.

964 Yu, M. (2011). Generation, function and diagnostic value of mitochondrial DNA copy number
965 alterations in human cancers. Life Sci *89*, 65–71.

966 Yu, H., Zhao, W., Xie, M., Li, X., Sun, M., He, J., Wang, L., and Yu, L. (2020). Real-Time
967 Monitoring of Self-Aggregation of β-Amyloid by a Fluorescent Probe Based on Ruthenium
968 Complex. Anal Chem *92*, 2953–2960.

969 Yu, J., Wang, Q., Chen, N., Sun, Y., Wang, X., Wu, L., Chen, S., Yuan, H., Xu, A., and Wang, J.
970 (2013). Mitochondrial transcription factor A regulated ionizing radiation-induced mitochondrial
971 biogenesis in human lung adenocarcinoma A549 cells. J Radiat Res *54*, 998–1004.

Zhang, T., Ikejima, T., Li, L., Wu, R., Yuan, X., Zhao, J., Wang, Y., and Peng, S. (2017). Impairment of Mitochondrial Biogenesis and Dynamics Involved in Isoniazid-Induced Apoptosis of HepG2 Cells Was Alleviated by p38 MAPK Pathway. Front Pharmacol *8*, 753.

977 **FIGURE LEGENDS**

978 **Figure 1. Generation of the dual-fluorescent protein reporter system**

979 (**A**) Schematic illustration of the pEGFP-cox8 reporter system.

980 (**B**) Schematic illustration of the pLVX-actin-mCherry reporter system.

981 (**C**) Live imaging of EGFP-Cox8-mCherry-Actin-HeLa cells within 16 hours. Arrow

982 points to the observed dynamic changes of cell proliferation.

983 (**D**) Confocal microscopy observation of co-localization of GFP-COX8 on the

984 mitochondria. The GFP-COX8-HeLa cells were stained with TMRE (200 nM) for 20

985 minutes before the examination by confocal microscopy. Scale bar: 10 μm.

986

987 **Figure 2. Verification of mitochondrial biogenesis phenomenon observed by the**

988 **dual fluorescence reporting system**

989 (**A**) The cells were treated with mitochondrial biogenesis inducer drug (AICAR, 0.5

990 mM) and observed using high-content imaging and screening (HCS) system after

991 different treatment hours. In the figures, green color indicates the mitochondria

992 encoding COX8-EGFP, red color shows the actin encoded by actin-mCherry, and blue

993 color represents the DAPI stained nuclei. Scale bar: 25 μm.

994 (**B**) The mean fluorescence intensity (MFI) ratios of HeLa cells treated by AICAR after

995 different hours, in comparison with the non-AICAR treated cells as the control group.

996 (**C**) Western blot (WB) assay for the HeLa cells which were treated with mitochondrial

997 biogenesis inducer drug (AICAR, 0.5 mM). Total proteins were extracted after 12 hours.

998 (**D**) The graph shows the comparison of the relative intensity for expressions of GFP

999 and mitochondrial biogenesis marker proteins between the non-AICAR treated group
1000 and the AICAR treated group. Bar graphs are presented as mean ± sd, n = 3.
1001
1002 **Figure 3. In-situ observation of the biological effects of gamma-radiation via the**
1003 **dual-fluorescence reporter system**
1004 (**A**) HeLa-cox8-EGFP-actin-mCherry cells were exposed to 1 Gy, 2 Gy, 4 Gy gamma-
1005 ray and incubated for 24 h and observed with confocal laser scanning microscope.
1006 Green color indicates the mitochondria encoding COX8-EGFP, red color shows the
1007 actin encoded by actin-mCherry, and blue color represents the DAPI stained nuclei.
1008 Scale bar: 25 μm.
1009 (**B**) The ratio comparison for the mean fluorescence intensity (MFI) of GFP over
1010 mCherry fluorescence intensities quantified in the Figure 3A. The MFI was determined
1011 by ImageJ software. Bar graphs are presented as mean ± sd, n = 3.
1012 (**C**) The cellular mean fluorescence intensity (MFI) measured by Thermo High Content
1013 Imaging and Screening (HCS) system. HeLa-Cox8-EGFP-actin-mCherry cells were
1014 exposed to 1 Gy, 2 Gy, and 4 Gy gamma-ray respectively. MFI changed with time after
1015 the γ-ray irradiation.
1016
1017 **Figure 4. Detection of the radiation effect on HeLa cells exposed to different**
1018 **radiation doses**
1019 (**A**) CCK-8 assay for cell viability.
1020 (**B**) LDH assay for cell cytotoxicity.

1021 (**C**) Colony formation assay of HeLa cells after 14 days under different radiation doses.

1022 (**D**) Flow cytometry results of Annexin V-PI assay.

1023 (**E**) Apoptotic cells at different radiation doses.

1024 (**F**) Cell cycle examination. The experiment was performed 3 times. Data are presented

1025 as Mean±SD; $P < 0.01$(**); $P < 0.001$(***); ns: not significant compared with untreated

1026 cells.

1027

1028 **Figure 5. Analysis of cytosolic ROS (cROS) evel and mitochondrial ROS (mROS)**

1029 **level after irradiation of the cells**

1030 (**A**) cytosolic ROS assessment using CellROX Green probe at 6 h.

1031 (**B**) mitochonrial ROS assessment using MitoSOX Red probe at 6 h.

1032 (**C**) The graph shows the representative MFI histogram of CellROX Green (cytosolic

1033 ROS production).

1034 (**D**) The graph shows the representative MFI histogram of MitoSOX (mitochondrial

1035 superoxide production). n = 500 cells calculated per group. Scale bar: 20 μm

1036

1037 **Figure 6. Analysis of mitochondrial membrane potential change after irradiation**

1038 **of the cells**

1039 (**A-B**) Mitochondrial membrane potential change was assessed by JC-1 staining at 12h

1040 after irradiation. JC-1 monomers (green) and aggregates (red) were detected by

1041 fluorescence microscopy (**A**) and flow cytometry (**B**). scale bars: 10 μm.

1042 (**C**) The graph shows the proportion of JC-1 monomers change with different irradiation

1043 doses.

1044

1045 **Figure 7. Comparative analysis of γ-H2AX and 53BP1 foci generated in the**

1046 **irradiated cells**

1047 (**A**) Representative images for DNA damage detection when the cells were exposed to

1048 radiation with different radiation doses. Green: γ-H2AX; red: 53BP1; Blue: DNA

1049 nucleus stained with DAPI; Scale bars: 10 μm.

1050 (**B**) The percentage of population with the noted number of γ-H2AX foci corresponding

1051 to the respective fluorescence images.

1052 (**C**) The percentage of population with the noted number of 53BP1 foci corresponding

1053 to the respective fluorescence images. At least 100 nuclei per genotype were used for

1054 quantification. Image auto-quantification was performed with CellProfiler version 4

1055 (www.cellprofiler.org).

1056

1057 **Figure 8. Radiation induces mitochondrial Ca^{2+} accumulation**

1058 (**A**) Photomicrograph shows the radiation induced change and cellular distribution of

1059 Ca^{2+} stained with Fluo-4 AM and mitochondrial calcium using Rhod-2 AM.

1060 (**B-C**) Bar diagram shows alteration in Ca^{2+} concentration in HeLa cells stained with

1061 Fluo-4 AM (5 μM) and Rhod-2 AM (1 μM), respectively, analyzed using fluorescence

1062 microscope and imaging by imageJ software. Images were captured under fluorescence

1063 microscope with 20X objective. n = 500 cells calculated per group. Scale bar: 20 μm.

1064 **Figure 9. Effects of intracellular ATP depletion by radiation**

1065 HeLa cells treated with different doses of radiation (0, 1, 2 and 4Gy). Quantitative
1066 analysis of intercellular ATP level in percentage. *P<0.05, **P<0.01 and ***P < 0.001
1067 indicated significant differences compared to non-treated cells group. All the results are
1068 presented as mean ± SD; n=3.
1069
1070 **Figure 10. Radiation interferes with mitochondrial function and mediates**
1071 **apoptosis**
1072 (**A**) Effect of gamma-gay irradiation on mitochondrial DNA copy number. HeLa cells
1073 were exposed to gamma-ray at doses of 1 Gy, 2 Gy and 4 Gy, respectively. After 6, 12,
1074 24 hours, total genomic DNA was extracted and used as a template to detect the
1075 mtDNA/ nDNA ratio by RT-qPCR. Data are presented as Mean±SD; #: significant
1076 compared with unirradiated group; $^{**}P < 0.01$; $^{***}P < 0.001$.
1077 (**B**) Effect of irradiation on the activity of citrate synthase (CS). HeLa cells were
1078 exposed to gamma-ray at doses of 1 Gy, 2 Gy and 4 Gy, respectively. After 6, 24 hours,
1079 the expression level of citrate synthase activity was detected by UV-Vis
1080 spectrophotometer.
1081 (**C**) Western blot assay of the related proteins after radiation treatment. HeLa cells were
1082 treated with different doses of irradiation (0, 1, 2, 4 Gy), and total proteins were
1083 extracted at different time points. The WB assay shows the changes of expression of
1084 mitochondrial biogenesis marker proteins (PGC-1α, p-AMPK, NRF1, TFAM and Mfn1)
1085 and apoptotic marker proteins (BAX, Bcl-2, CytoC, Caspase-3, Cleaved Caspase-9,
1086 PARP) with time.

1087

1088 **Figure 11. Mitophagy activity assessed using mKeima in HeLa cells**

1089 Elevated levels of mitophagy were observed following irradiation with 1 Gy, 2 Gy, 4

1090 Gy after 9 hours. AICAR (0.5mM) and mitophagy inhibitor (CsA, 50 nM) were also

1091 applied as the positive and negative controls. n = 500 cells calculated per group. Scale

1092 bar: 20 μm.

1093

1094 **Figure 12. Analysis of mitochondrial biogenesis and apoptosis**

1095 (**A**) Analysis of EGFP/mCherry ratio in High Content Screening (HCS) at 6 h.

1096 (**B**) Analysis of EGFP/mCherry ratio in High Content Screening (HCS) at 12 h.

1097 (**C**) Analysis of EGFP/mCherry ratio in High Content Screening (HCS) at 24 h.

1098

1099 **Figure 13. Schematic diagram of biochemical events after ionizing radiation**

1100

1101 **Figure 1**

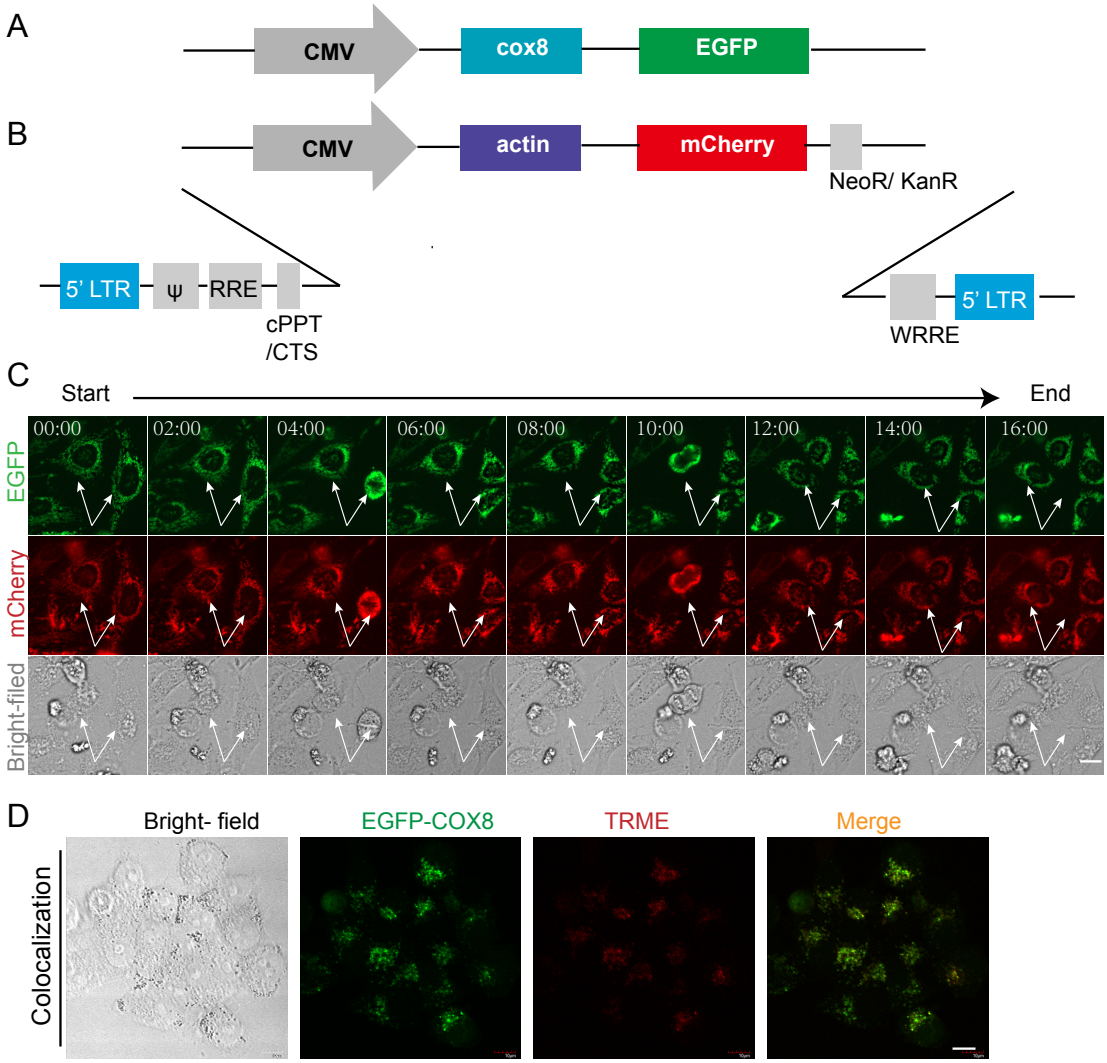

1102

1103

1104 **Figure 2**

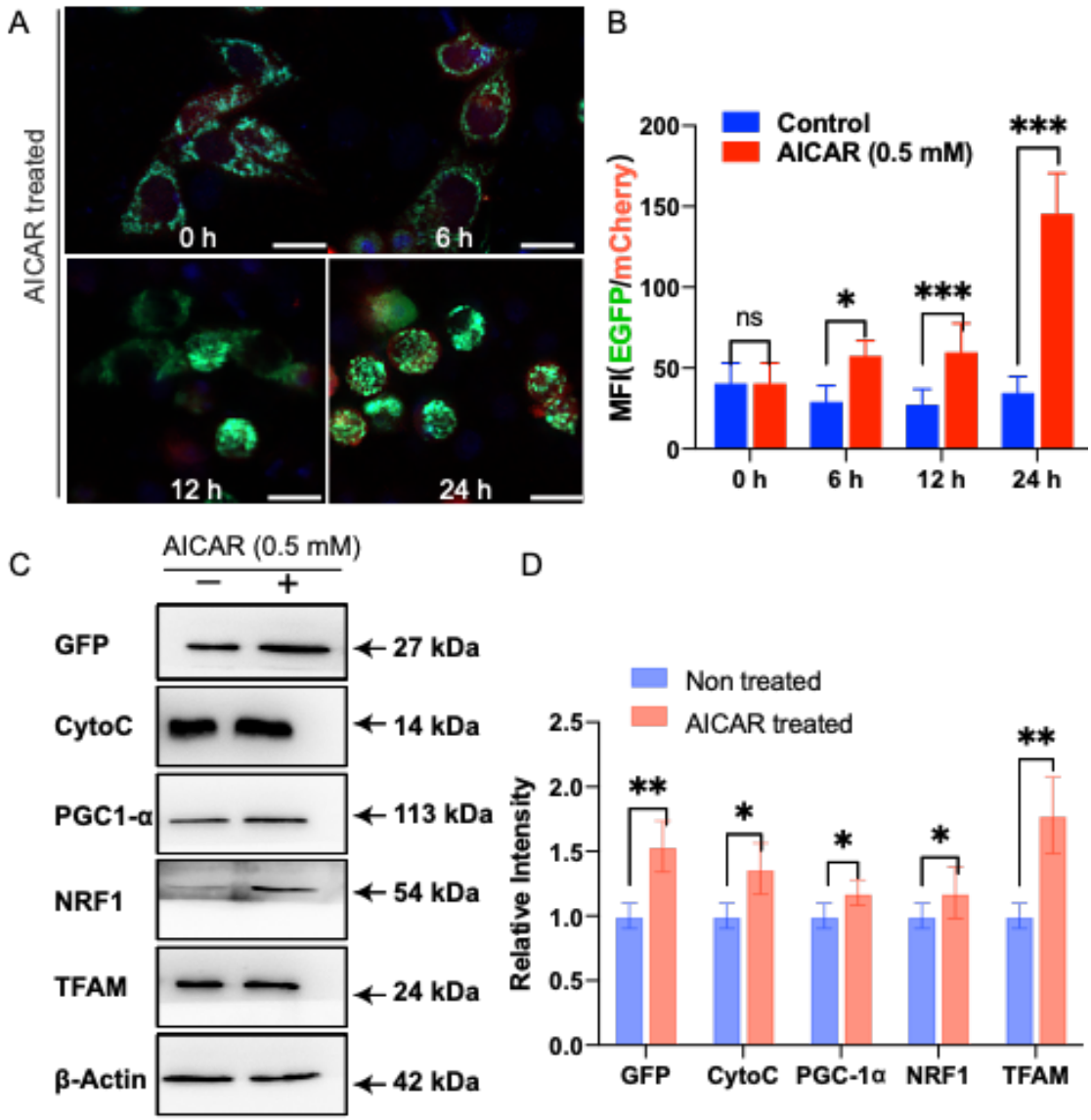

1105

1106

1107 **Figure 3**

1108

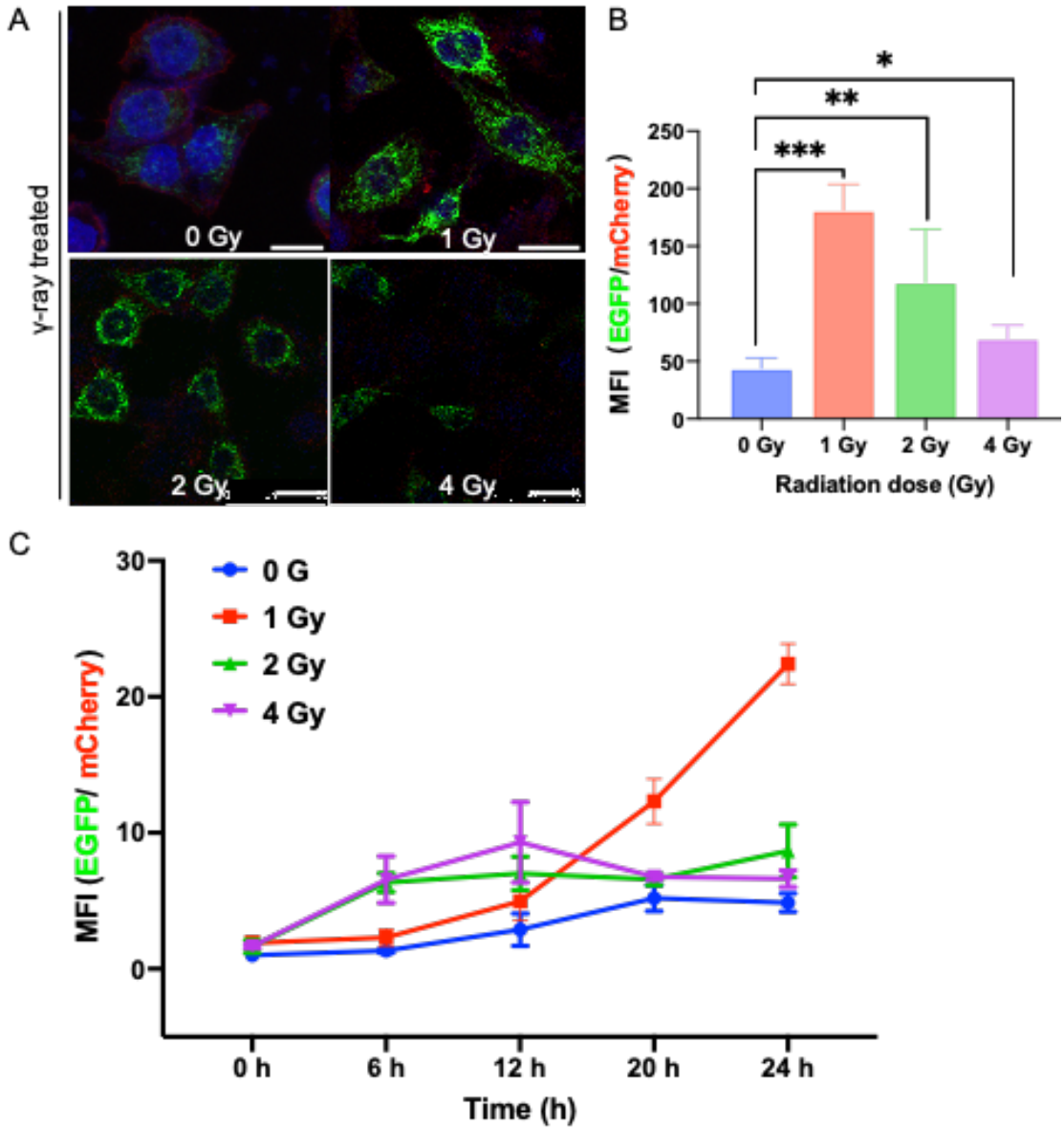

1109

1110

1111 **Figure 4**

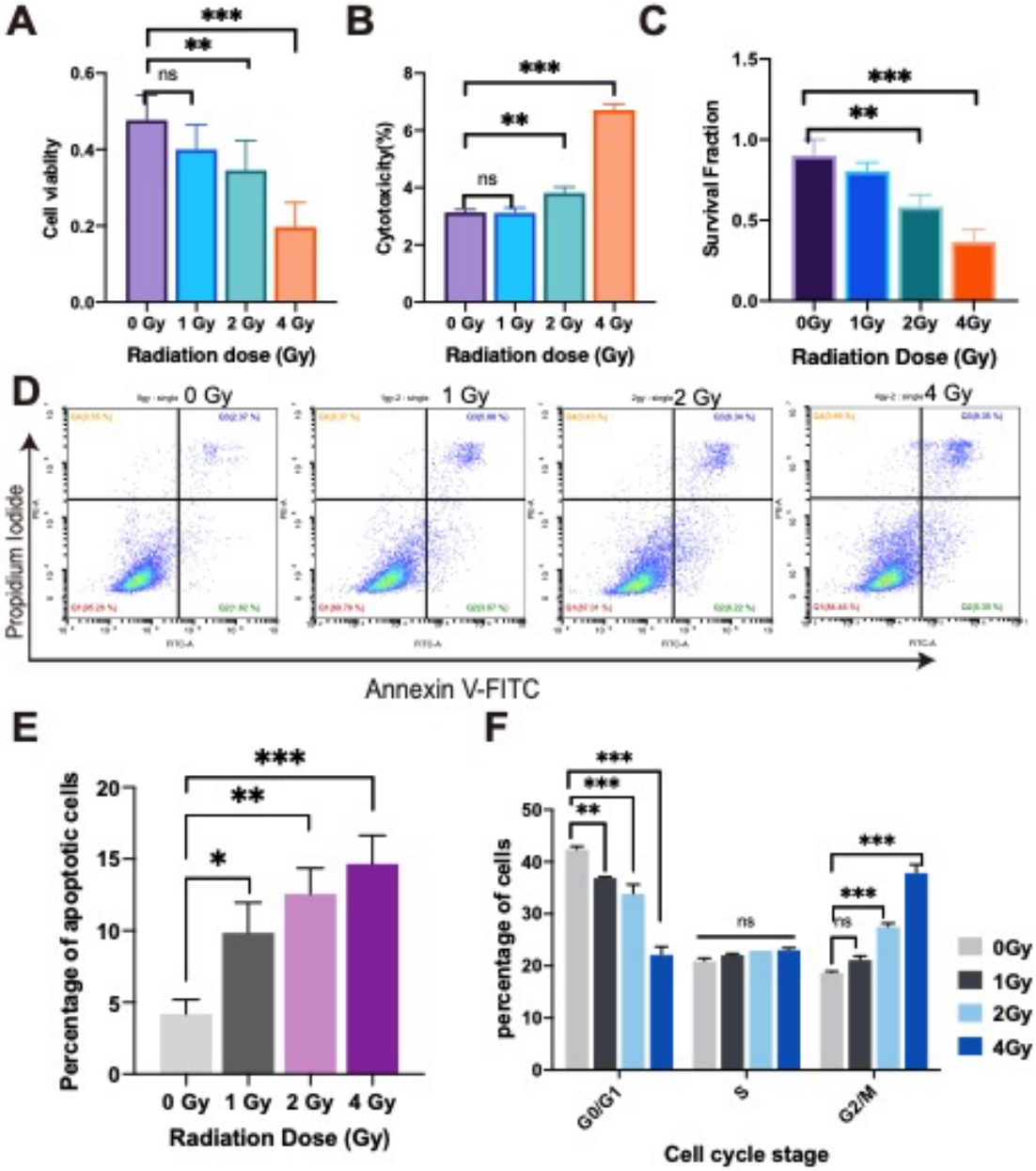

1112

1113

1114

1115 **Figure 5**

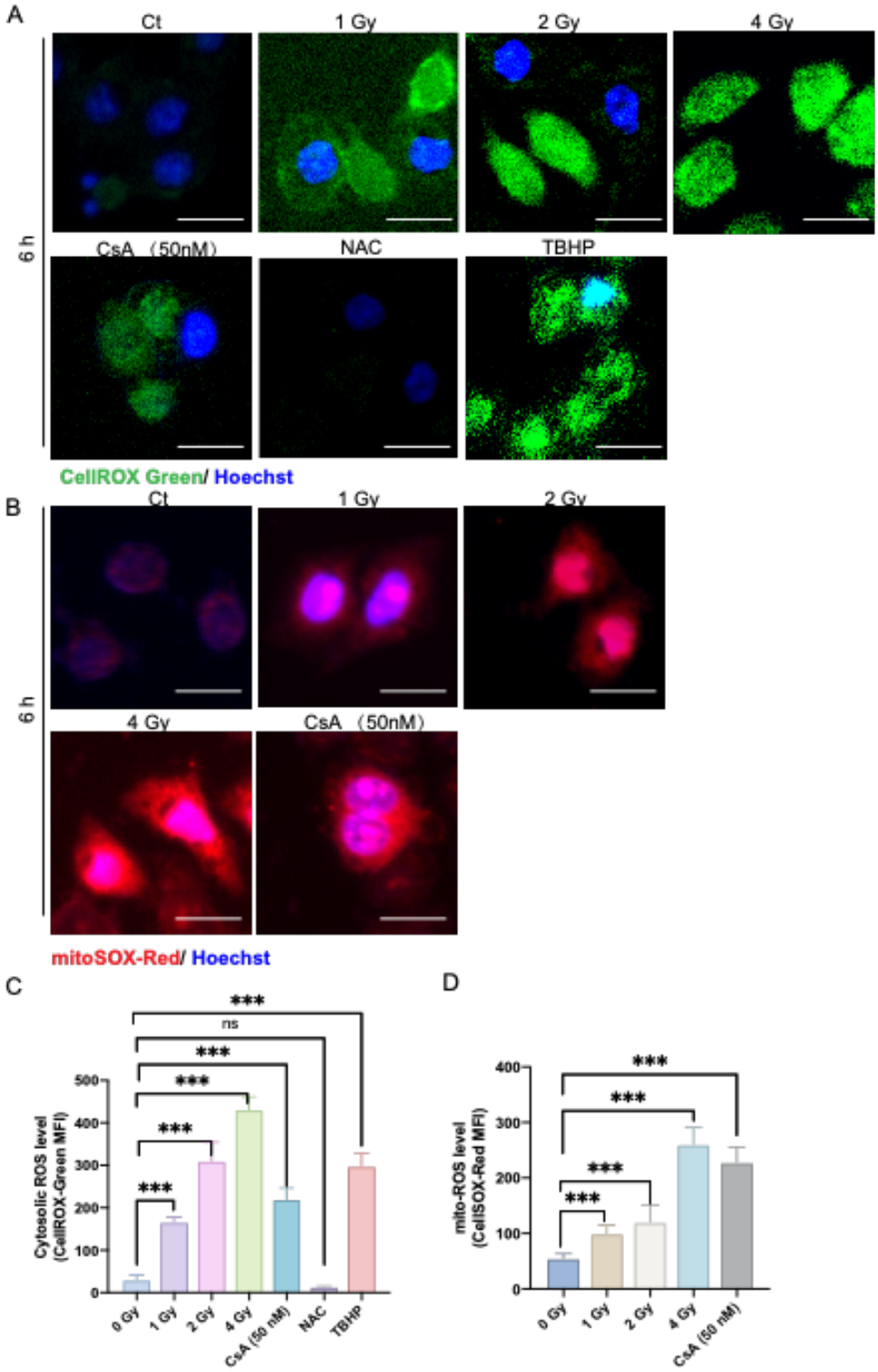

1116

1117

1118 **Figure 6**

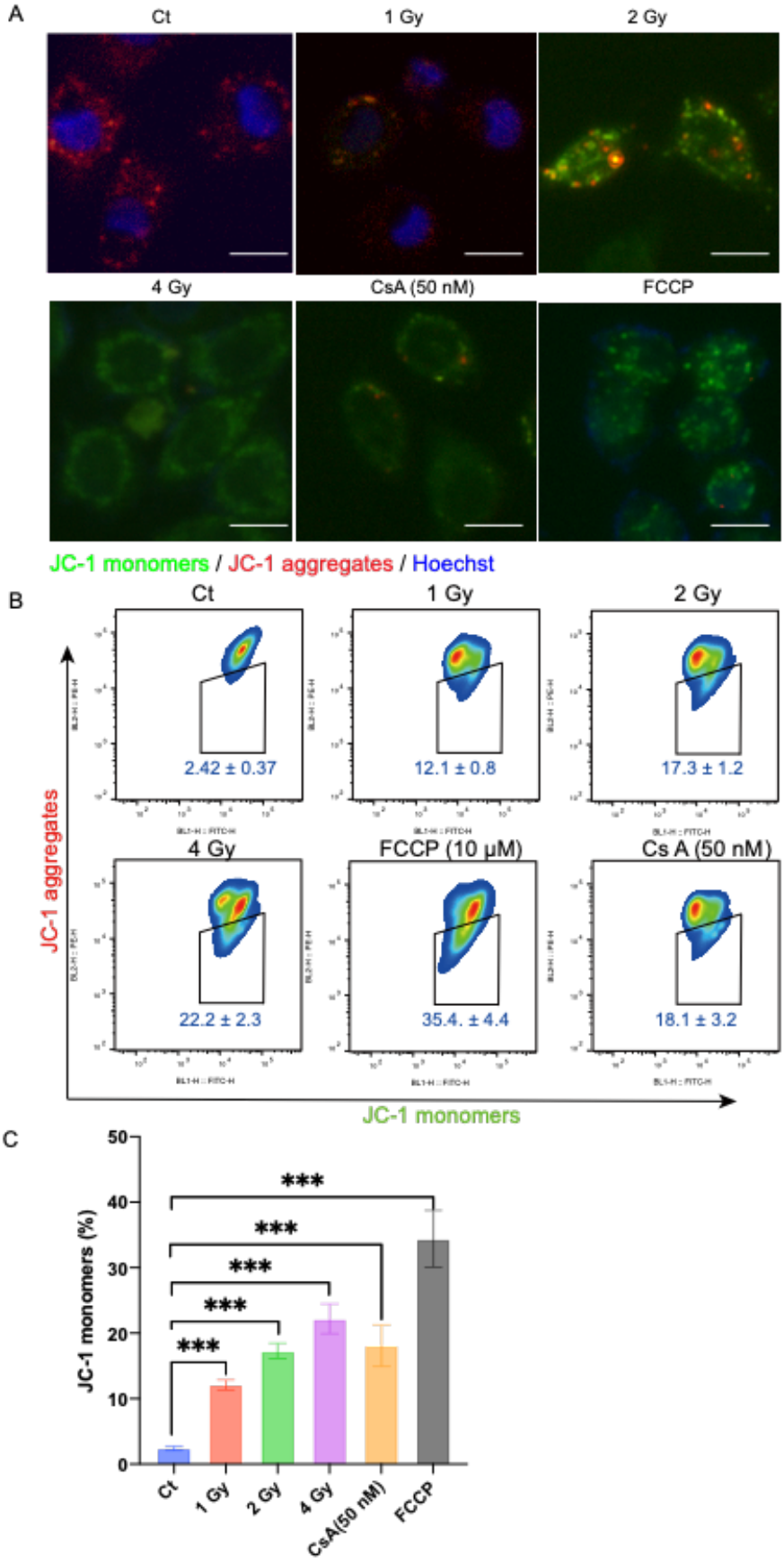

1119

1120 **Figure 7**

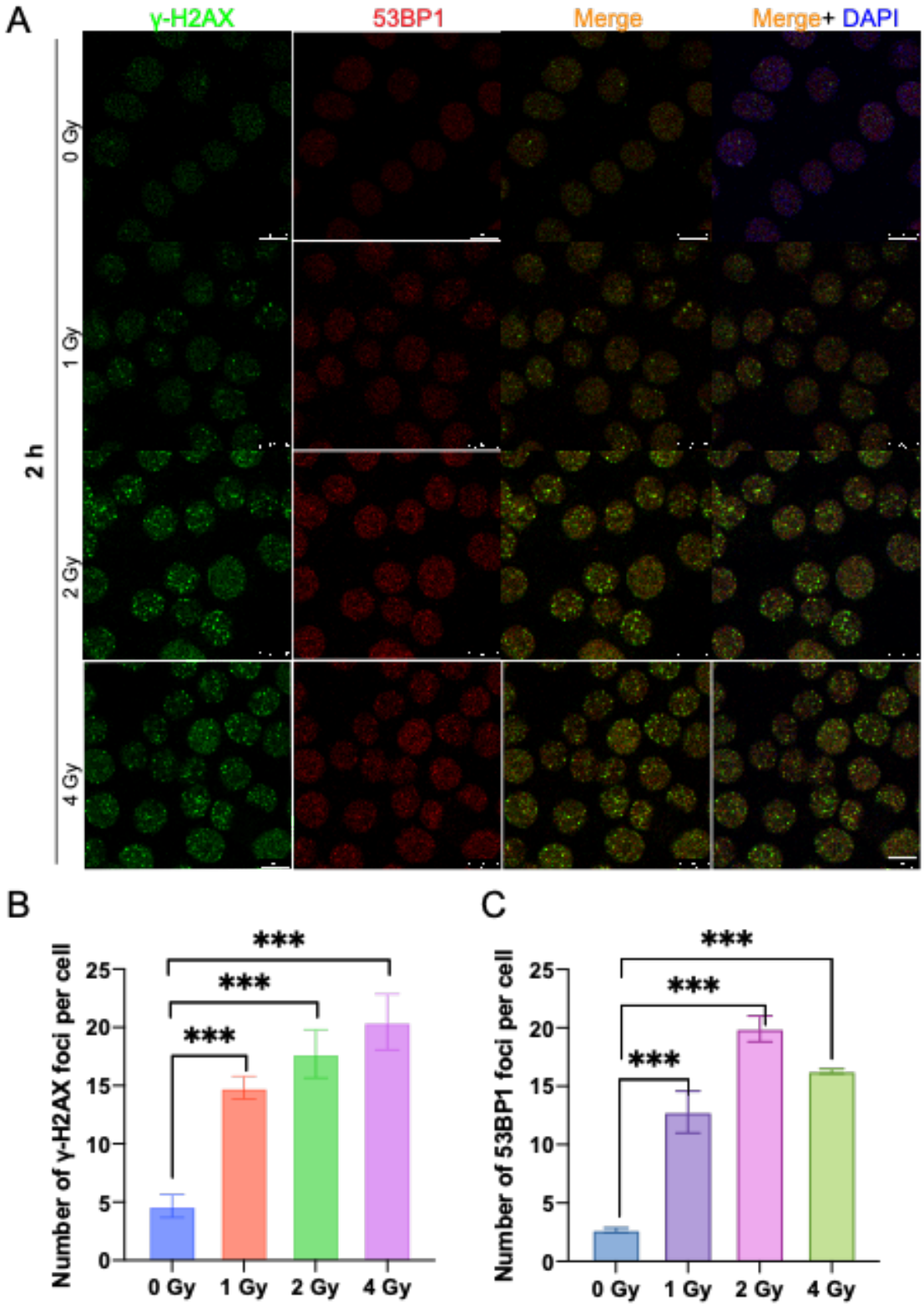

1121

1122

1123

Figure 8

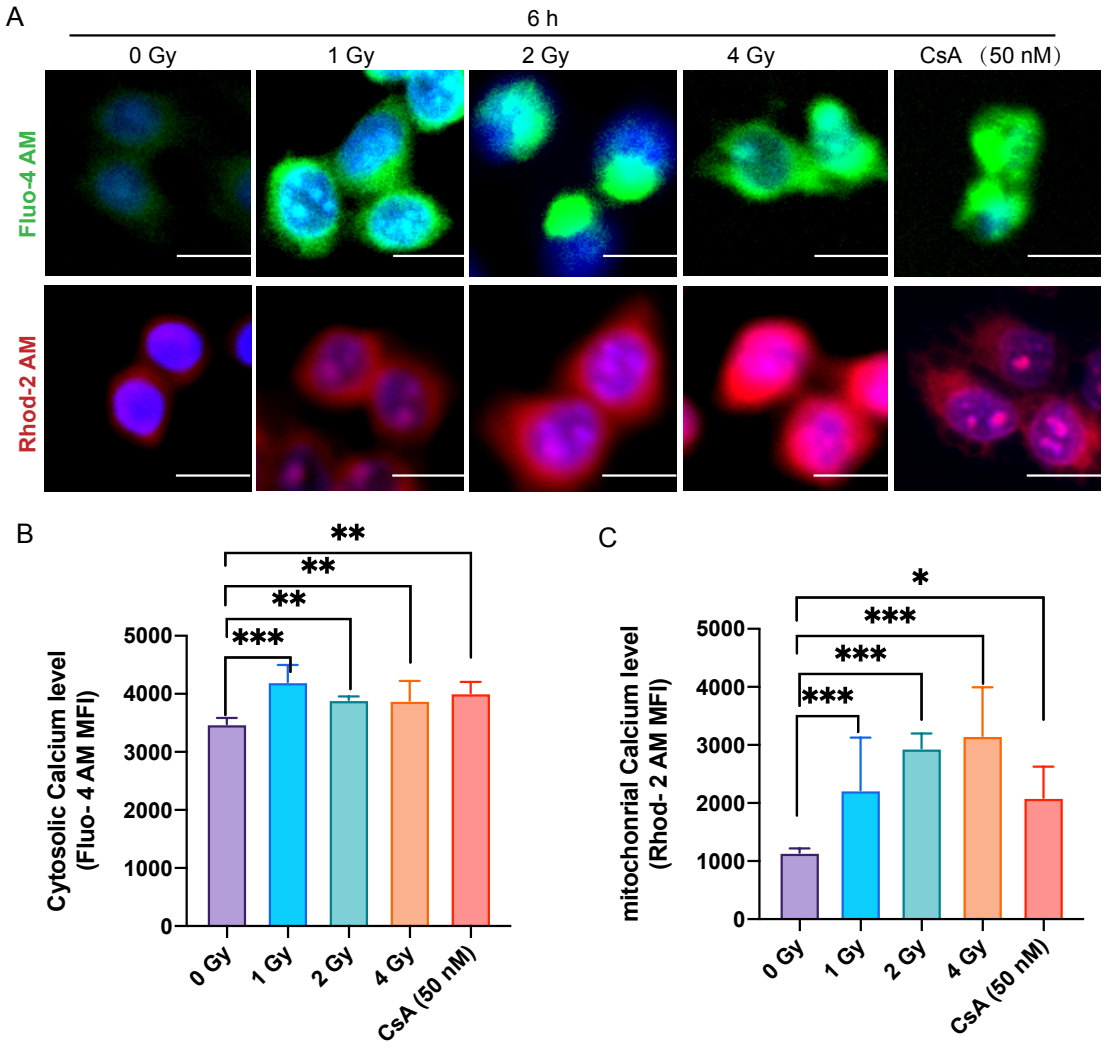
A
6 h
0 Gy
1 Gy
2 Gy
4 Gy
CsA （50 nM）
Fluo-4 AM
Rhod-2 AM
B
Cytosolic Calcium level
(Fluo- 4 AM MFI)
5000
4000
3000
2000
1000
0
***
**
**
**
0 Gy
1 Gy
2 Gy
4 Gy
CsA (50 nM)
C
mitochonrial Calcium level
(Rhod- 2 AM MFI)
5000
4000
3000
2000
1000
0
***
***
***
*
0 Gy
1 Gy
2 Gy
4 Gy
CsA (50 nM)

1127 **Figure 9**

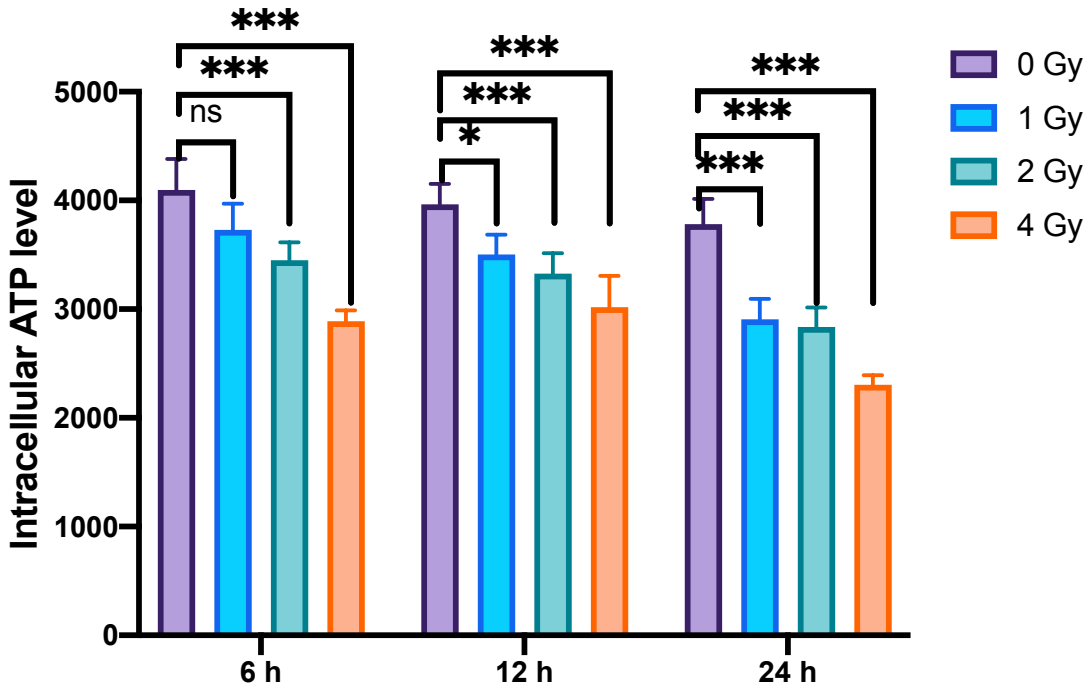

1128

1129

1130 **Figure 10**

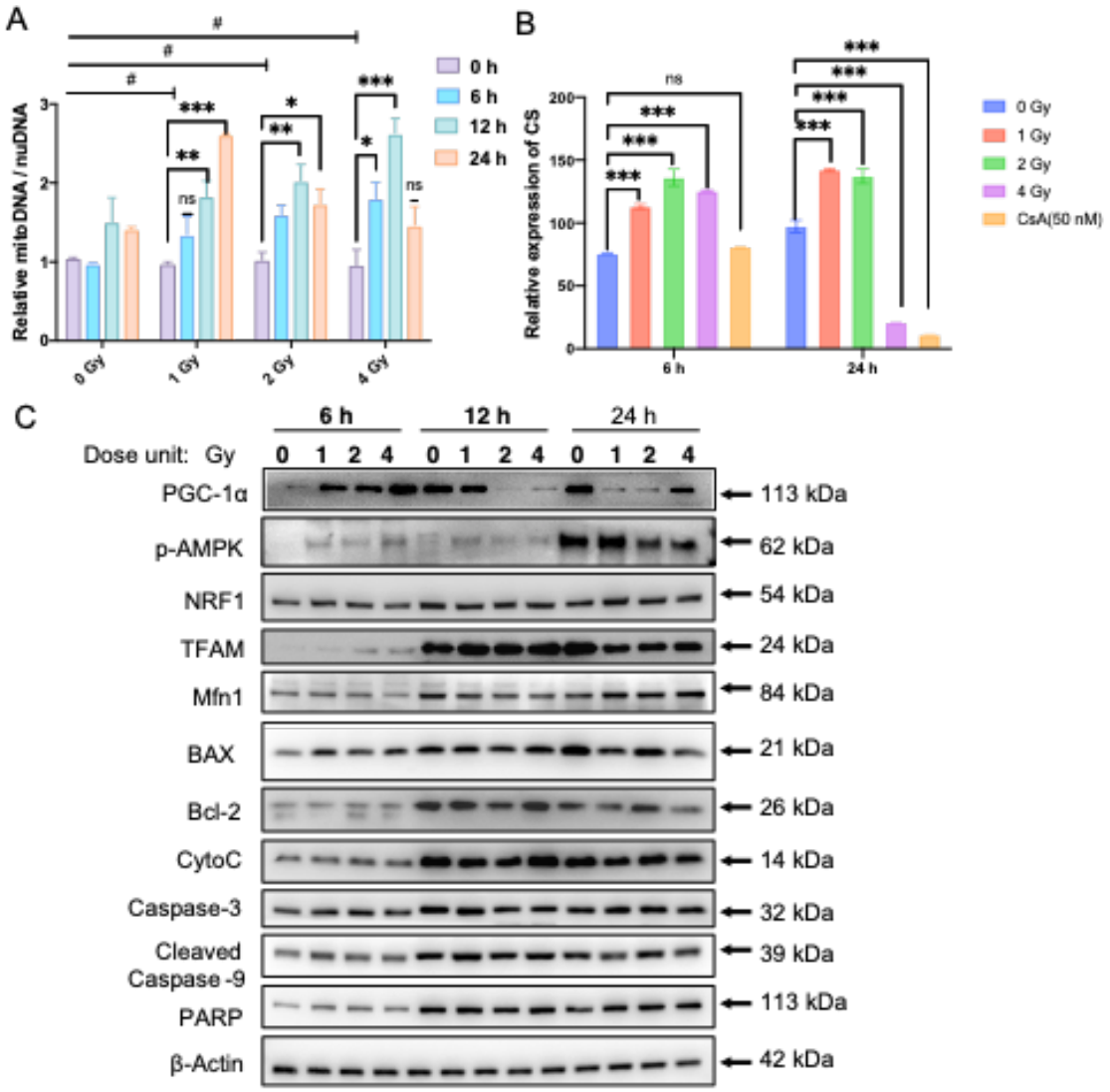

1131

1132

1133

1134 **Figure 11**

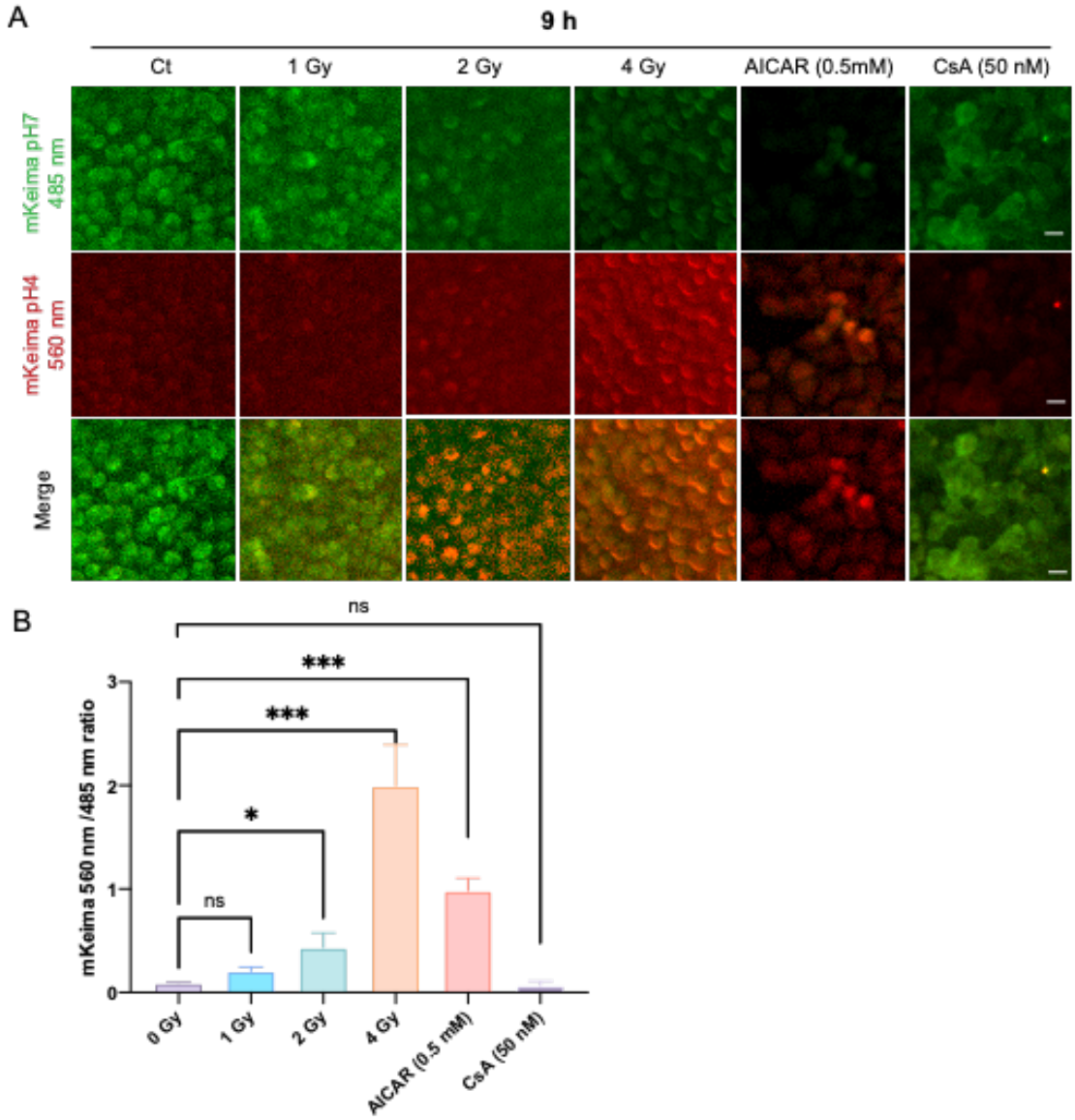

1135

1136

1137 **Figure 12**

1138

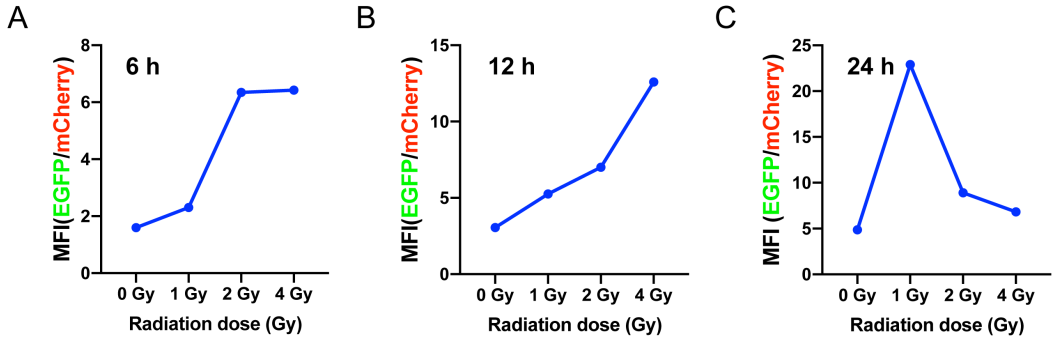

1139

1140

1141 **Figure 13**

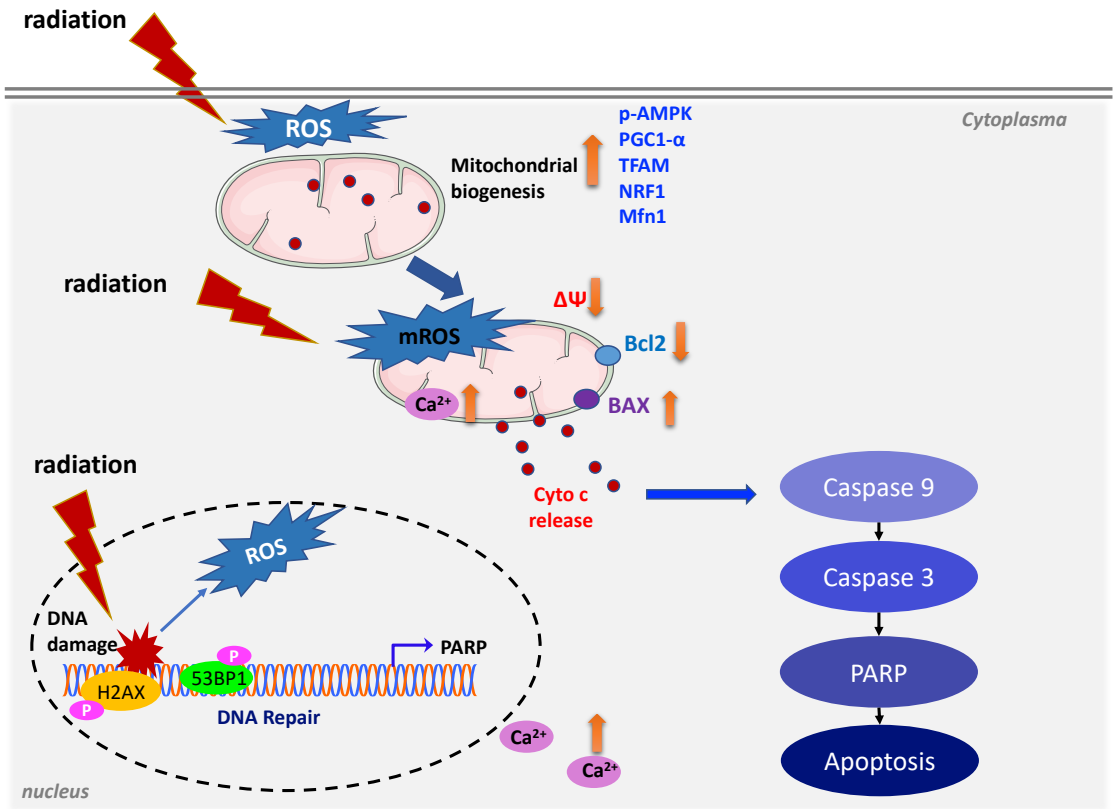

1142

Supplementary Information

Table S1

Oligonucleotides for amplify PCR product of COX8

Oligonucleotides	Sequence 5′ → 3′	size (bp)
Oligo1	CTAGAGATCTGGTACCGTCGAC TGCAGAGATCCGCTAGGGG TACTCCGTGCCATCATGTCC GTCCTGACGCCGCTGCTGC TGCGGGGCTTGACAGGCTC GGCCCGGCGGCTCCCAGTG CCGCGCGCCAAGATCCATT CGTTGCCGCCGGAGGGG	154
Oligo2	AGCTTCCCCTCCGGCGGCAACG AATGGATCTTGGCGCGCGG CACTGGGAGCCGCCGGGC CGAGCCTGTCAAGCCCCGC AGCAGCAGCGGCGTCAGG ACGGACATGATGGCACGGA GTACCCCTAGCGGATCTCT GCAGTCGACGGTACCAGAT CT	155

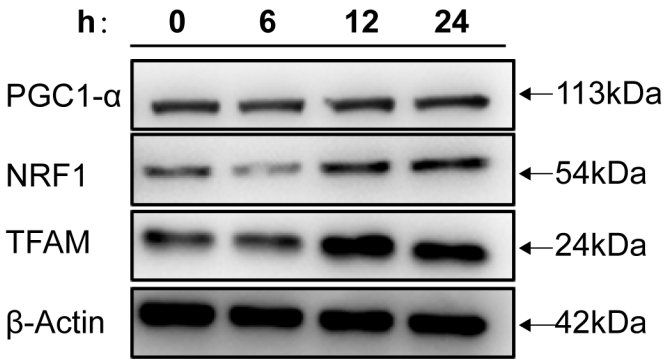

Figure S1. Western blot assay for verifying the effect of AICAR on mitochondrial biogenesis

HeLa cells were treated with mitochondrial biogenesis inducer drug (AICAR, 0.5 mM), and the whole cell extracts were collected at different time points. The mitochondrial biogenesis marker proteins (PGC-1α, NRF1 and TFAM) are indicated in the plot.

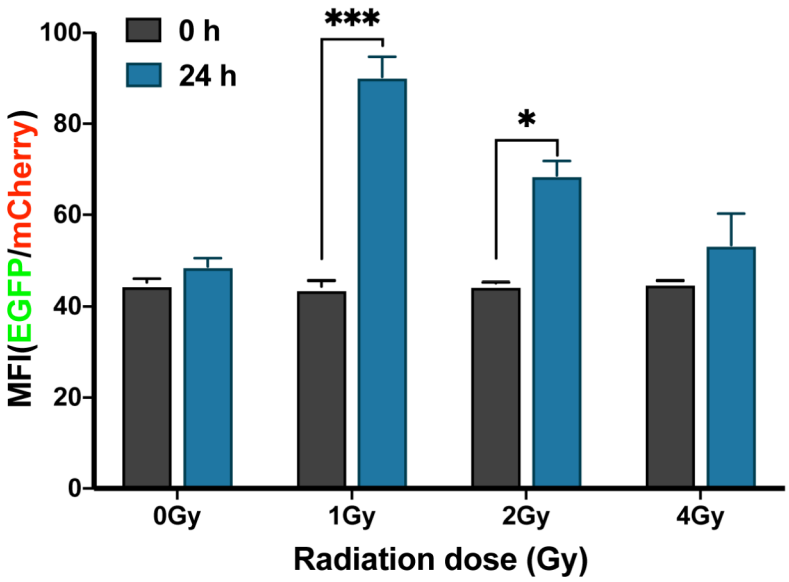

Figure S2. The mean fluorescence intensity (MFI) was determined by flow cytometry for the HeLa cells with or without irradiation.

HeLa-cox8-EGFP-actin-mCherry cells were exposed to 1 Gy，2 Gy，4 Gy gamma-ray and incubated for the indicated periods. The analysis and comparison MFI obtained from the dual-fluorescent measurements by flow cytometry.

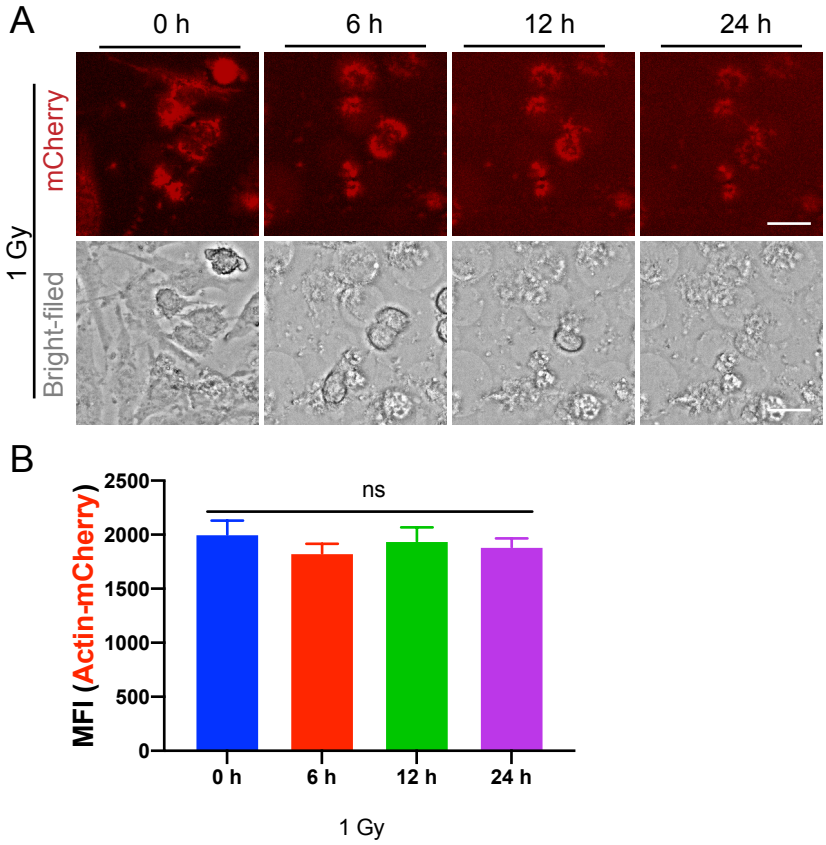

Figure S3. The mean fluorescence intensity (MFI) of Actin-mCherry was determined by living fluorescence microscopy for the HeLa cells with with or without irradiation (1 Gy).

(**A**) Fluorescence images and bright field images were taken at 0, 6, 12 and 24 hours after irradiatied with 1 Gy dose.

(**B**) The histogram is the statistical chart of the mean fluorescence intensity of Actin-mCherry.

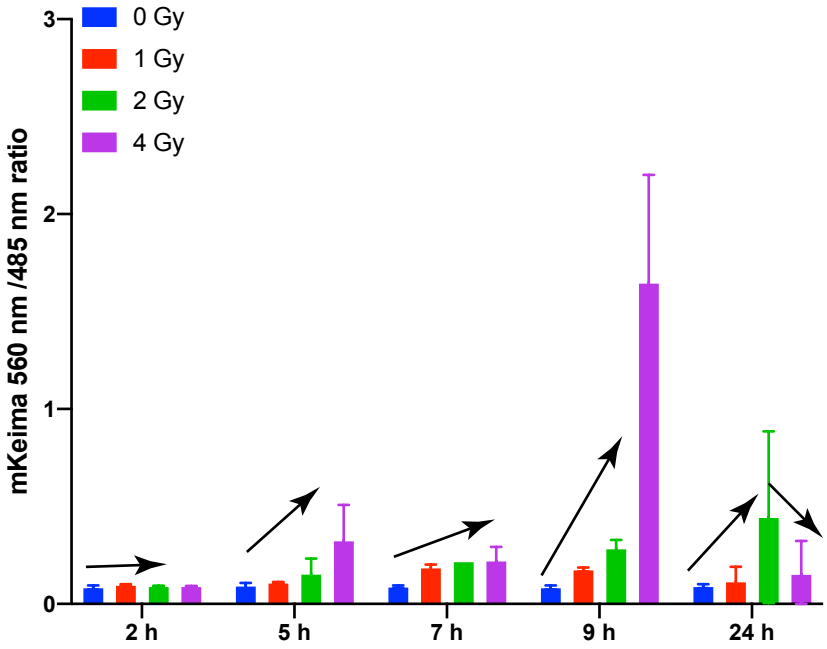

Figure S4. Mitophagy activity assessed using mt-Keima in HeLa cells

Elevated levels of mitophagy were observed following irradiation with 1 Gy, 2 Gy, 4 Gy. The fluorescence ratio of red fluorescence to green fluorescence (560 nm/ 485 nm) at different time points (2, 5, 7, 9 and 24 hours) was calculated by high content fluorescence analysis system. n = 1000 cells calculated per group.

S1 Video

S2 Video

S3 Video

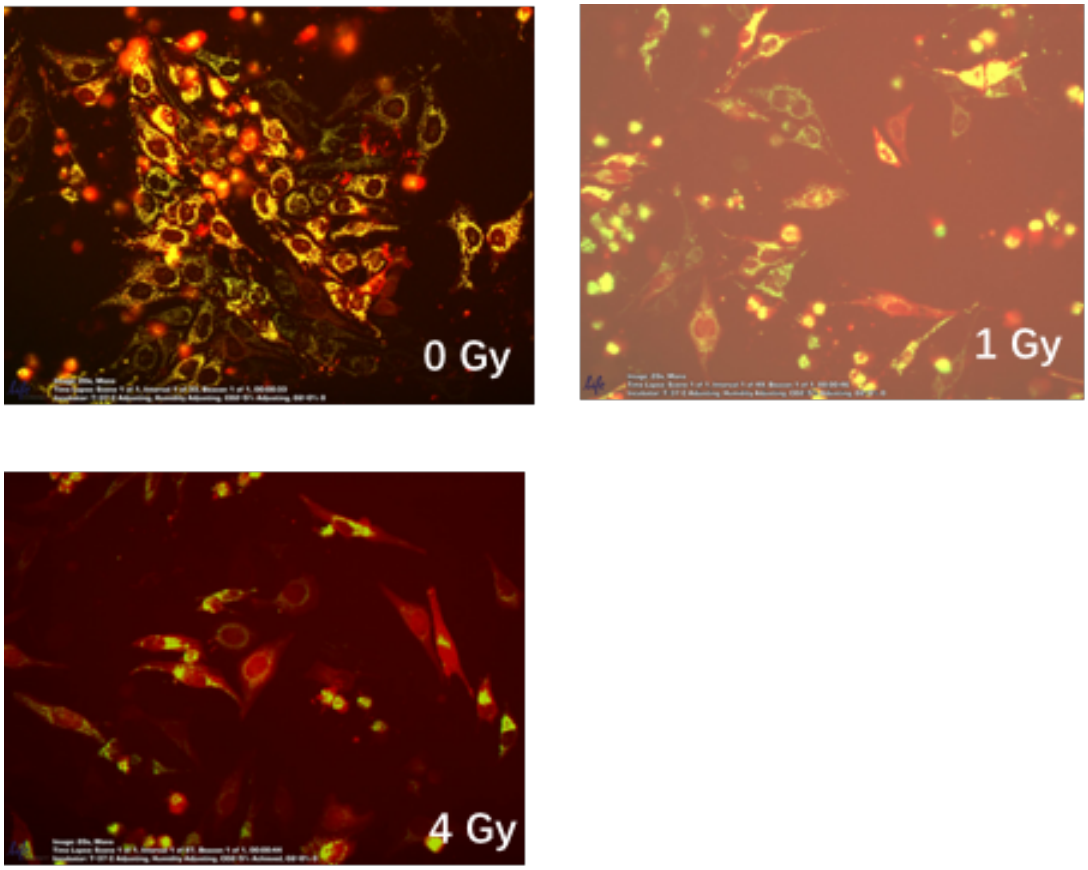

In-situ real-time video of dual fluorescence reporter system of irradiated cells (Video S1, Video S2, Video S3)